Universidad de Buenos Aires
Facultad de Ciencias Exactas Y Naturales
Departamento de Computación

Clasificación Automática de Naranjas utilizando Técnicas de Data Mining y Procesamiento de Imágenes

Tesis presentada para obtener el título de
Magíster en Explotación de Datos y Descubrimiento de Conocimiento

Juan Pablo Mercol

Directora de Tesis: María Juliana Gambini

Buenos Aires, 2010

CONTENTS

LIST OF FIGURES

LIST OF TABLES

ABSTRACT

Las técnicas de data mining consisten en la extracción de información a partir de una gran cantidad de datos, mediante el descubrimiento de patrones y regularidades por medio de algoritmos de aprendizaje automático entre otros. Esto puede aplicarse a la clasificación de objetos por medio de imágenes.

En la cadena de producción de frutas, el control de calidad es realizado por personas entrenadas, que examinan los frutos mientras éstos avanzan por una cinta transportadora. Luego los clasifican en distintas categorías de acuerdo a diversas características visuales.

En este trabajo presentamos un método para clasificar naranjas por medio de imágenes. El proceso consiste en capturar las imágenes mediante una cámara digital para luego extraer características y entrenar diversos algoritmos de data mining, los cuales deberán clasificar a la naranja en una de las tres categorías pre-establecidas.

Los algoritmos de data mining utilizados son cinco diferentes árboles de decisión (J48, Classification and Regression Tree (CART), Best First Tree, Logistic Model Tree (LMT) y Random Forest), tres redes neuronales (Perceptrón Multicapa con Backpropagation, Radial Basis Function Network (RBF Network), Sequential Minimal Optimization para Support Vector Machines (SMO)) y una regla de clasificación (1Rule).

Uno de los principales problemas que tiene la clasificación de naranjas es la detección del cáliz, debido a que en las imágenes el cáliz puede confundirse con un defecto. Por lo tanto, previo a la extracción de características necesitamos detectar y remover el cáliz de la imagen. Para ello, en la etapa de segmentación utilizamos el espacio de color CIE L*a*b* y análisis de agrupamiento k-medias para identificar las regiones candidatas que puedan pertenecer al cáliz o a un defecto. Luego, realizamos la extracción de características utilizando momentos de Zernike y análisis de componentes principales para obtener diversos descriptores para cada región. Por último, en la etapa de clasificación empleamos diversos algoritmos de aprendizaje automático (tres redes neuronales y un árbol de decisión) mediante los cuales clasificamos a la región como cáliz o defecto.

Los resultados obtenidos son alentadores, debido a la buena precisión alcanzada por los clasificadores, lo que demuestra la factibilidad de construir un sistema de clasificación de naranjas basado en técnicas de data mining y procesamiento de imágenes, para ser utilizado en la industria alimenticia.

ABSTRACT

Data mining can be summarized as the discovery of patterns and regularities from large amounts of data, using machine learning algorithms among others. These methods can be applied to object recognition and classification using image processing techniques.

In fruits and vegetables production lines, the quality assurance is performed by trained personnel who inspect the fruits while they travel over a conveyor belt, and classify them in a number of categories based on visual features.

In this thesis we present an automatic orange grading system, which uses artificial visual inspection to extract features from images captured using a digital camera. With these features, we train several data mining algorithms, which should classify the fruits in one of the pre-established categories.

The data mining algorithms used are five different decision trees (J48, Classification and Regression Tree (CART), Best First Tree, Logistic Model Tree (LMT) and Random Forest), three artificial neural networks (Multilayer Perceptron with Backpropagation, Radial Basis Function Network (RBF Network), Sequential Minimal Optimization for Support Vector Machines (SMO)) and a classification rule (1Rule).

Prior to feature extraction, we have to detect and remove the stem-end or calyx from the image, in order not to misclassify the calyx as a defect in the classification step. To do so, we use the CIE L*a*b* color space and perform K-means clustering in the segmentation step to identify candidate regions where a calyx or a defect could be found. Then, we perform feature extraction using Zernike moments and Principal Component Analysis to retrieve several descriptors of each region. Finally, we use several classification algorithms (Multilayer Perceptron, Radial Basis Function Network, Sequential Minimal Optimization for SVM and Logistic Model Tree) for the classification step, in order to classify the region as calyx or defect.

The obtained results are promising because of the good accuracy obtained by the classifiers, which shows the feasibility of building an orange grading system based on image processing and data mining techniques to be used in the food industry.

1. INTRODUCTION

1.1 ***Motivation***

During the last years, there has been an increase in the need to measure the quality of several products, in order to satisfy customers needs in the industry and services. In fruit and vegetable production lines, the quality assurance is the only step which is not done automatically. For oranges, quality assurance is performed by trained personnel who inspect the fruits while they travel over a conveyor belt, and classify them in a number of categories based on visual features.

Performing an accurate classification is crucial in order to fulfill the quality requirements established by several organizations to allow the commercialization of the fruits for specific markets. If a good quality orange is misclassified as defective or intermediate, it will be sold at a lower price, but if a defective orange is misclassified as good, it might lead to the application of fines for selling defective oranges as good; or if the defect is an illness, it can lead to discard the whole lot of fruits, causing considerable loss.

In the industry, there are very few automatic classification machines, mainly because of the need of advanced image processing. This is required to perform fast and complex analysis given the wide range of variations found on natural products [37].

Visual aspect is very important for fruits. An orange with an excellent peel is sold at a higher price than another orange with the same internal features but with superficial defects. This promoted the establishment of quality standards at many organizations For instance, Zubrzycki & Molina [17] present a table with five categories for oranges, lemons and tangerines. This can be seen in Table 1.1.

However, the differences in quality categories are diffuse and subjective, therefore two orange grading experts can classify the same specimen into different categories. It is possible to reduce this subjectivity by using an automatic classifier.

Defect type \ Categories	Extra	Cat. I	Cat. II	Cat. III	Cat. IV
Serious defects	0%	2%	3%	4%	4%
Deep damage	0%	3%	5%	5%	5%
Overripe	0%	1%	3%	9%	9%
Total serious	0%	3%	5%	9%	9%
Deform	0%	1%	10%	20%	100%
Kind of mark					
Diffuse Level 1	5%	20%	40%	100%	100%
Diffuse Level 2	0%	5%	20%	50%	100%
Deep Level 1	0%	15%	20%	3%	100%
Deep Level 2	0%	3%	10%	20%	10%
Total marks	5%	25%	40%	100%	100%
TOTAL	5%	25%	40%	100%	100%

Tab. 1.1: Citrus classification categories. Adapted from [17]

1.2 ***State of the Art***

In the scientific community, there is significant interest in the development of artificial vision based fruit classification systems. Recce et. al [37] introduce an orange classifier which uses artificial neural networks and Zernike polynomials. Unay and Gosselin [10] show an apple classifier based on color and texture features, using principal components analysis and neural networks. Fobes [28] proposes a system to estimate the volume of a fruit from digital images. Morimoto et al. [56] introduce a system for fruit shape recognition using the fractal dimension and neural networks.

One of the main complications faced by the authors is the detection of the calyx, because it can be wrongly classified as a defect [37]. Another difficulty is the speed needed to perform the classification, because it has to be done in the time imposed by the speed of the conveyor belt.

Several authors have studied stem-end/calyx detection with success. Unay and Gosselin extract several features (invariant moments of Hu, textural features of Haralick, Gray-Level Co-occurrence Matrices, averages and ranges of coefficients of Daubichies wavelet decomposition, averages and ranges of intensities of objects) and then compare two classifiers (K-Nearest Neighbor and Support Vector Machines) [11]. Recce et. al introduce a stem detection system based on Zernike moments and Neural Networks [37]. Ruiz et. al present a system which uses color segmentation and Bayesian decision rules to discriminate the calyx and cut stem [34]. Leeman and Destain propose a pattern matching by correlation approach to detect the calyxes and stem-ends. Xing, Jancsok and Baerdemaeker

perform Principal Component Analysis (PCA) for stem end/calyx detection of apples, where they analyze the contour features of the first principal component score images [20].

In this thesis, we present a method to classify oranges using digital still images. The process consists of the extraction of relevant features to be able to classify the orange into three categories (good, intermediate and defective). Some of the most relevant features used are statistical descriptors, histogram analysis, and the fractal dimension (FD), which can be used to characterize the oranges' peel smoothness as a quality indicator.

The method developed in this thesis is exclusively focused in the calyx detection and classification steps, but in order to make this thesis self contained, in chapter 3 we briefly introduce the system that should be used to capture the images.

The results of this thesis have been presented in [25], [23] and [24].

1.3 ***Thesis Organization***

This thesis is organized in the following way: we start by presenting the fundamentals of digital image processing and data mining in chapter 2, where we explain in detail all the machine learning algorithms used in this thesis. In chapter 3, a general description of the system is made, introducing the image capture step.

Next, the calyx detection subsystem is analyzed in chapter 4, where we explain the segmentation process, the feature extraction algorithms involved, and the classification of candidate regions as calyx or defect using data mining algorithms.

In chapter 5 we focus on the quality categories classification subsystem, explaining how the features used by the data mining algorithms in the classification step are obtained, and in section 5.2 we present the classification results obtained with the experiments.

Finally, in chapter 6 we present the conclusions and future works.

2. PRELIMINARIES

In this chapter we introduce the fundamentals of digital image processing and data mining in order to give the reader a background on these techniques and make this thesis self containing. If the reader has knowledge on these concepts, this chapter could be skipped.

2.1 ***Digital Image Processing***

2.1.1 ***Digital Image Representation***

An image can be represented as a two dimensional function $f : \mathbb{R}^2 \rightarrow \mathbb{R}$, $f(x, y)$, being x and y the spatial coordinates and the value of f at a certain point is the intensity of the image in that point. A digital image is an image $f : \mathbb{N} \times \mathbb{N} \rightarrow [0, 1, ..., L-1]$ where L is the luminance value [49]. The processing of this kind of images is named 'Digital Image Processing'.

A digital image is represented in a computer as a two dimensional matrix where each element is called a 'Picture Element' or 'Pixel'. The value of each pixel can represent a gray level, a chromatic value or it can also represent a non-human visual magnitude like an infrared image [49].

Figure 2.1 (a) shows a 15x15 pixels binary (black and white) image and Figure 2.1 (b) shows its computer representation, where white is represented with 1 and black with 0.

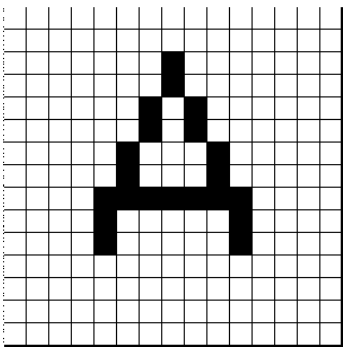

(a) 15x15 pixels binary image

1	1	1	1	1	1	1	1	1	1	1	1	1	1	1
1	1	1	1	1	1	1	1	1	1	1	1	1	1	1
1	1	1	1	1	1	1	0	1	1	1	1	1	1	1
1	1	1	1	1	1	1	0	1	1	1	1	1	1	1
1	1	1	1	1	1	0	1	0	1	1	1	1	1	1
1	1	1	1	1	1	0	1	0	1	1	1	1	1	1
1	1	1	1	1	0	1	1	1	0	1	1	1	1	1
1	1	1	1	1	0	1	1	1	0	1	1	1	1	1
1	1	1	1	0	0	0	0	0	0	0	1	1	1	1
1	1	1	1	0	1	1	1	1	1	0	1	1	1	1
1	1	1	1	0	1	1	1	1	1	0	1	1	1	1
1	1	1	1	1	1	1	1	1	1	1	1	1	1	1
1	1	1	1	1	1	1	1	1	1	1	1	1	1	1
1	1	1	1	1	1	1	1	1	1	1	1	1	1	1
1	1	1	1	1	1	1	1	1	1	1	1	1	1	1

(b) 15x15 pixels binary image representation

Fig. 2.1: Binary image and its computer representation

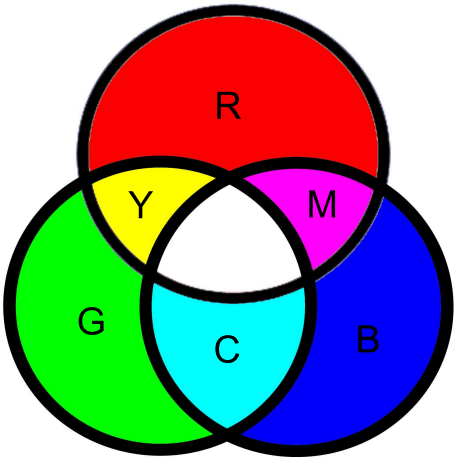

Fig. 2.2: Additive model of light: Adding Red and Green forms Yellow, Red and Blue form Magenta, Blue and Green form Cyan and adding Red, Green and Blue form white

Color images can be represented in different ways, according to the color space being used. This will be explained in the following section.

2.1.2 ***Color Spaces***

Color images are represented as a combination of matrices where each matrix represent a single color component image.

- **Red, Green and Blue (RGB) Color Space**: Red, Green and Blue are the colors basis of light, so it is widely used in image acquisition using photo and video cameras, and also for displaying images in computer monitors and projectors. An example of additive colors is shown in Figure 2.2. A RGB image consists of three components: Red, Green and Blue, so each pixel has three values. This can be seen in Figure 2.3. Figure 2.4 shows the Red, Green and Blue components of an image of size 144x192 with 8 bits per channel (or component), so each pixel can contain 256 (2^8) levels for each component.

- **Cyan, Magenta, Yellow, Black ($CMYK$) Color Space**: Cyan, Magenta and Yellow are the colors basis for pigments, and the secondary colors of light, because they subtract the color from the reflected light. For example, Cyan is the absence of Red, Magenta the absence of Green and Yellow the absence of Blue [49]. An example of subtractive colors is shown in Figure 2.5.

  The formula to convert from RGB to CMY is shown in Equation (2.1).

  Theoretically, equal amounts of pigments of cyan, magenta and yellow should produce black, but in practice it produces a kind of gray, so black (K) is also added [49].

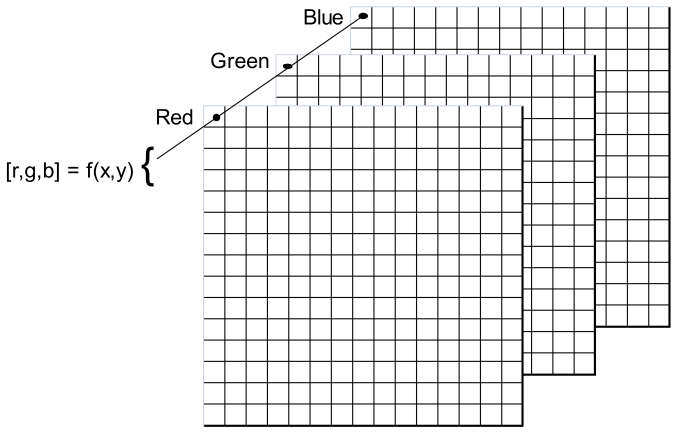

Fig. 2.3: RGB image made of three layers.

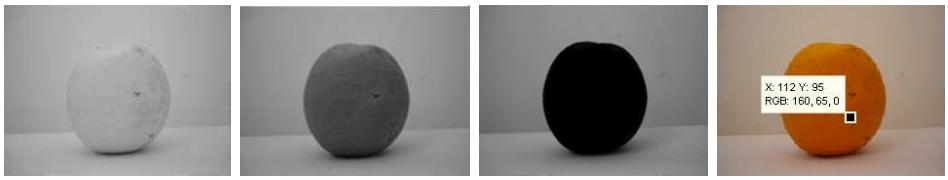

(a) Component R (b) Component G (c) Component B (d) RGB with 1 píxel

Fig. 2.4: Red, Green and Blue (RGB) components of an image.

$$\begin{bmatrix} C \\ M \\ Y \end{bmatrix} = \begin{bmatrix} 1 \\ 1 \\ 1 \end{bmatrix} - \begin{bmatrix} R \\ G \\ B \end{bmatrix} \tag{2.1}$$

- **Hue, Saturation, Value (HSV) Color Space**: The HSV color space consists of three components:
  - Hue: Can be considered similar to tint, and it is expressed as an angle of the color hexagon considering Red as 0°.
  - Saturation: Represents the purity of the color, and is expressed as the distance from the center of the hexagon to the point of interest.
  - Value: Is the amount of light of a certain color. A value of 0 is black, and a value of 1 in the center of the hexagon is white.

  The conversion from RGB to HSV is done by mapping the RGB values which are in cartesian coordinates, to HSV values which are in cylindrical coordinates [49]. An example of the HSV Color Space is shown in Figure 2.6.

- **CIE XYZ colorspace**: The CIE XYZ color space, which stands for 'Commission Internationale de l´Eclairage' (International Commission on Illumination) XYZ, consists of a linear transformation of the RGB color space using Equation (2.2) [33].

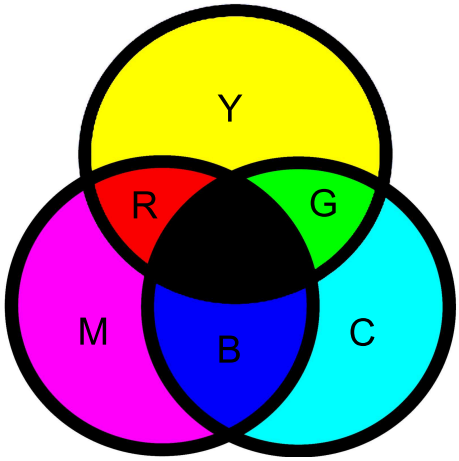

Fig. 2.5: Subtracting Colors of light: Subtracting magenta and cyan from white forms blue, subtracting magenta and yellow from white forms red, subtracting cyan and yellow from white forms green, and subtracting cyan, magenta and yellow forms black

$$\begin{bmatrix} X \\ Y \\ Z \end{bmatrix} = \begin{bmatrix} 0.6079 & 0.1734 & 0.2000 \\ 0.2990 & 0.5864 & 0.1146 \\ 0.0000 & 0.0661 & 1.1175 \end{bmatrix} \cdot \begin{bmatrix} R \\ G \\ B \end{bmatrix} \tag{2.2}$$

- **CIE L*a*b* colorspace**: The CIE L*a*b* color space was designed to be perceptually uniform, so it is considered as one of the best color spaces for matching the human perception distance of colors [14].

  The color space consists of three layers:

  - Luminance or brightness layer $L*$: Can have the range from 0 to 100, where 0 is black and 100 white. It does not contain color information.
  - Red-Green chromatic layer $a*$
  - Blue-Yellow chromatic layer $b*$ [26]

  An example of CIE L*a*b* components is shown in Figure 2.7, where 2.7 (a) shows the luminance component of the image, 2.7 b) and 2.7 c) show the a and b components and Figure 2.7 d) shows both the a and b components which include all the color information, discarding the luminance information.

  CIE L*a*b* is based on the XYZ color space, so conversion from RGB to CIE L*a*b* is performed with the following equations: First, convert from RGB to XYZ using Equation (2.2).

  Then, convert from XYZ to L*a*b* using Equation (2.3).

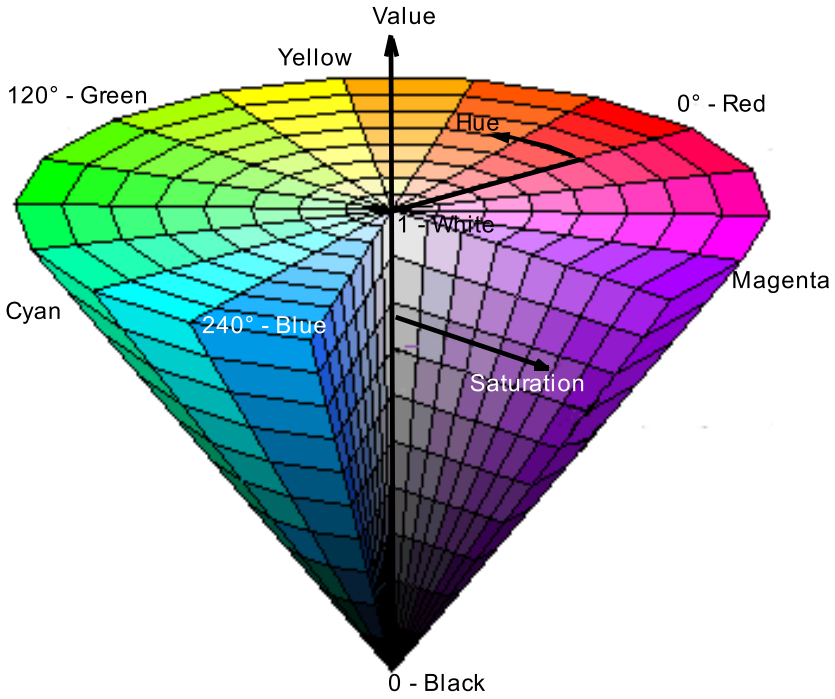

Fig. 2.6: HSV Color Space.

$$
\begin{aligned}
a* &= 500 * [f(X/X_n) - f(Y/Y_n)] \\
b* &= 200 * [f(Y/Y_n) - f(Z/Z_n)] \\
L* &= \begin{cases} 116 * (Y/Y_n)^{1/3} - 16 & \text{when } (Y/Y_n) > 0.008856, \\ 903.3 * (Y/Y_n) & \text{otherwise.} \end{cases}
\end{aligned}
\tag{2.3}
$$

where X_n, Y_n and Z_n are the values of reference for white (e.g.: $X_n = 1$, $Y_n = 0.9872$ and $Z_n = 1.18225$) [33].

(a) *L*uminance (b) Component $a*$ (c) Component $b*$ (d) Components $a*$ & $b*$

*Fig. 2.7: L*uminance, $a*$ and $b*$ (CIE L*a*b*) components of an image

2.1.3 *Morphological operators*

Morphological operators are primarily used with binary images to recover shapes of the image, which may be needed to describe the shape of the objects of interest [49].

In this section we explain the basic morphological operators used in this thesis.

- **Dilation**: Dilation consists in growing the objects by expanding their boundaries in a controlled way using a *structuring element*, which is the shape used to perform the operation [49]. The mathematical equation is the following:

$$G \oplus M = \{p : M_p \cap G \neq \oslash\}. \tag{2.4}$$

  where M is the set of non-zero mask pixels known as the structuring element, G is the original image consisting of the set of all non zero pixels of the matrix, p is the reference pixel (generally the center of the structuring element) and M_p is the structuring element shifted to the reference point p [21].

  The equation means that dilation of G using M results in all structuring elements which overlap with G at least in one point [49].

  An example of dilation operation can be seen in Figure 2.8 (c).

- **Erosion**: Erosion is the opposite to dilation, as the object is 'shrunk' or 'thinned' instead of grown. It also uses a structuring element, and the equation is denoted by:

$$G \ominus M = \{p : M_p \cap G^c \neq \oslash\ \}. \tag{2.5}$$

  which means that the resulting object will have a foreground value (e.g.: 1) in the center of the structuring element (p) only when it does not overlap with the background [49].

  An example of erosion is shown in Figure 2.8 (d).

- **Opening**: Morphological opening of G by M consists of performing erosion of G by M and that result dilated by M. In mathematical notation, opening is denoted by:

$$G \circ M = (G \ominus M) \oplus M \tag{2.6}$$

  and the result of morphological opening is an object which has been removed all the regions that cannot contain the structuring element M. Opening is commonly used to remove background noise, smooth object contours, break thin connections and remove thin protrusions [49].

  An example of the application of morphological opening operation is shown in Figure 2.8 (e), where it can be seen that the three regions in white are kept.

- **Closing**: Closing consists of dilation followed by erosion and the mathematical equation is the following:

$$G \bullet M = (G \oplus M) \ominus M \tag{2.7}$$

(a) Original image with background removed

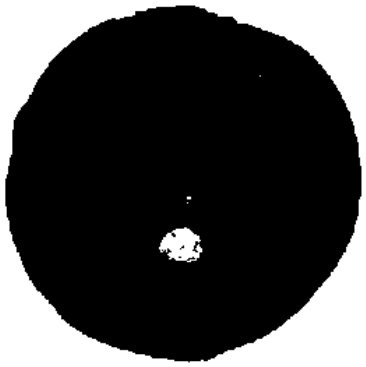

(b) Binary representation of the image

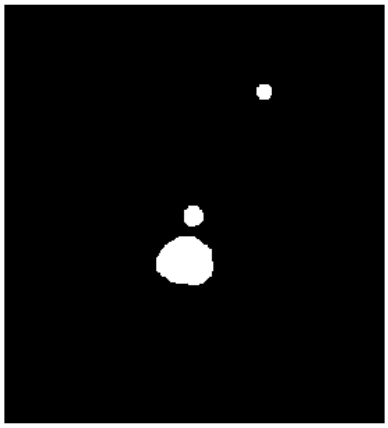

(c) Morphological dilation

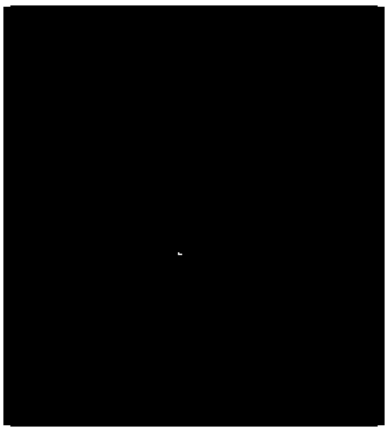

(d) Morphological erosion

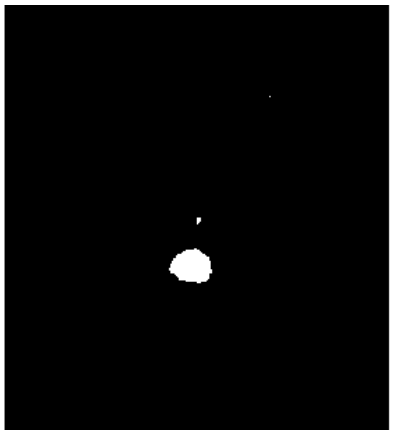

(e) Morphological closing

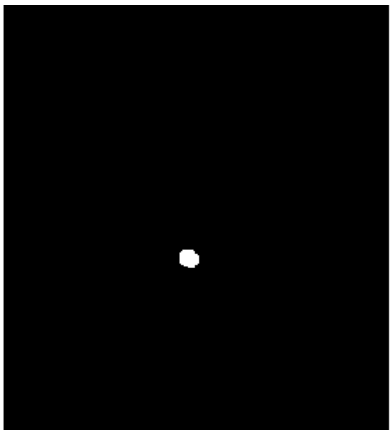

(f) Morphological opening

Fig. 2.8: Morphological operators

and similar to opening, closing smooths contours. However, it joins narrow breaks, fills long thin gulfs and fills holes smaller than the structuring element M [49].

An example of applying the closing operation is shown in Figure 2.8 (f), where it can be seen that only the biggest of the three regions is kept, as closing fills holes smaller than the structuring element, in which in this case has a size of 8 pixels and a circular shape.

Closing and opening can also be combined and are commonly used to remove noise.

2.2 *Data Mining and Knowledge Discovery in Databases*

Data mining can be defined as the discovery of patterns and regularities from large amounts of data, using machine learning algorithms among others. Another definition of Data mining given by [18] is:

> 'Data mining is the extraction of implicit, previously unknown, and potentially useful information from data.'

Data mining involves learning in a practical, not theoretical, way, where existing data takes the form of examples, and the output of the process is the prediction of new examples [18].

Data mining is also one step in the Knowledge Discovery in Databases (KDD) process. The steps involved in the KDD process are the following [16]:

1. **Data Cleaning**: Remove inconsistencies and noise.
2. **Data Integration**: Consolidate in a single data source data spread over different databases.
3. **Data Selection**: Irrelevant data for the task is discarded.
4. **Data Transformation**: Data are transformed for mining like performing aggregations or summarizations.
5. **Data Mining**: the process of discovering patterns and regularities from data, using machine learning algorithms among others.
6. **Pattern Evaluation**: the data mining step may generate several patterns or models, which should be evaluated in order to keep the most interesting ones. A pattern is considered interesting if it is valid on new data, it is potentially useful and novel [16]. Jan & Kamber [16] also mention that a pattern is interesting if it is easily understood by humans, something that for us is desirable, but depending on the task involved, it may not be so necessary and several machine learning algorithms like neural networks, which are very difficult to interpret by humans, are widely used.
7. **Knowledge Representation**: The representation of the discovered knowledge to the user, where information visualization techniques are applied.

Data mining is commonly used as a predictive tool, or as a descriptive tool used to describe the properties of the data [16]. The main functionalities of data mining are the following [16]:

- **Characterization and description**: Data characterization consists in describing the general features of the elements of a class, like for example describing the

characteristics of oranges that belong to CAT I. Data discrimination resides in describing classes by comparing a class against other different classes and computing the differences.

- **Association analysis**: Resides in finding attribute-value relations that occur together. It is mainly used in market basket analysis and transaction data analysis. Association rules are used for this purpose. For example, an association rules analysis in a supermarket may find that sausages and hot dog bread are bought together with a confidence of 90% (the probability of buying both items together) and a support of 30% (30% of all the transactions contains both).

- **Classification and prediction**: Classification consists in finding a model (using training data) that describes the data and when a new example with an unknown class is input, its class is predicted. Classification is explained in section 2.2.1.

- **Cluster analysis**: Cluster analysis consists in grouping similar elements in a cluster. It uses unsupervised learning because the nature of the class of the elements is not known in advance.

- **Outlier analysis**: Outliers are data elements that differ considerably from the rest of the elements in the dataset. In most cases outliers are a result of noisy or incorrect data, or it might be a valid value which, depending on the task, it might be worthwhile to analyze. For example, outliers are commonly used when detecting frauds.

- **Evolution analysis**: can be applied to all the previous items when dealing with objects with time variant behavior, such as stock market trends, where time-series analysis is commonly used.

2.2.1 ***Classification using machine learning algorithms***

In order to associate the features of the image with the corresponding class (good, intermediate or defective), we use several data mining Algorithms. For this purpose, we experiment with most of the algorithms available in the Waikato Environment for Knowledge Analysis (WEKA) software which are suitable for the kind of problem presented in this thesis, and choose the ones with the highest accuracy.

The chosen algorithms are: five different decision trees (J48, Classification and Regression Tree (CART), Best First Tree, Logistic Model Tree (LMT) and Random Forest), three artificial neural networks (Multilayer Perceptron with Backpropagation, Radial Basis Function Network (RBF Network), Sequential Minimal Optimization for Support Vector Machines (SMO)) and a decision rule (1Rule).

Before giving the definition of classification, we have to define some concepts like 'class' and 'hypothesis' in order to fully understand the following paragraphs.

There exist three definitions for class:

1. Classes as labels for different populations: in this case, members of each population are assigned to different classes, and membership to that group is not in question (e.g. dogs and cats). The allocation to a certain class, which is done by the supervisor, is independent of the attributes [41].

2. Classes are the result of a prediction problem: For example, to determine if tomorrow will rain (class = 1) or not (class = 0). This class is predicted based on knowledge of the attributes [41].

3. The class is a function of the attributes: For example, to determine if an item is faulty, there exists a rule which already classified items as faulty if certain attributes are out of a certain limit [41]. The goal is to create a rule which resembles the original one.

In our problem, we consider the class as a function of the attributes (definition N° 3) because there exists a rule used by the people who manually classify the fruit, and this rule is the one that has to be mimicked.

According to [41], classification can be related to supervised and unsupervised learning. In unsupervised learning, given a set of observations, the algorithm has to group the instances into classes or clusters based on similarity criteria [16]. On the other hand, in supervised learning we already know the class c of each observation in the dataset D of size m. The aim is to find a hypothesis or rule, h, that satisfies c for the members of D and will be a good guess for c when we have to classify a new observation [44], [41].

Another important aspect in machine learning is concept learning. In machine learning, the concept is 'the thing to be learned ' [18]. According to [36], Concept Learning means to infer a boolean-valued function from training examples of its input and output, so it can be seen as a searching problem through a predefined space of potential hypothesis to determine the hypothesis which best fit the training examples.

Figure 2.9 (a) shows an instance space example which consists of points in the x,y plane. In Figure 2.9 (b), a hypotheses consisting of lines is able to separate the classes but one instance is misclassified. Figure 2.9 (c) shows an hypothesis consisting of a parabola, which can perfectly classify the instances without error.

Overfitting: One important aspect that has to be considered when building machine learning algorithm is overfitting, which is a very common pathology of induction algorithms [8, 41].

Overfitting occurs when inferring more structure from the training set than is justified by the population from which it is drawn [41]. These added components do not improve accuracy when tested with new data samples [8].

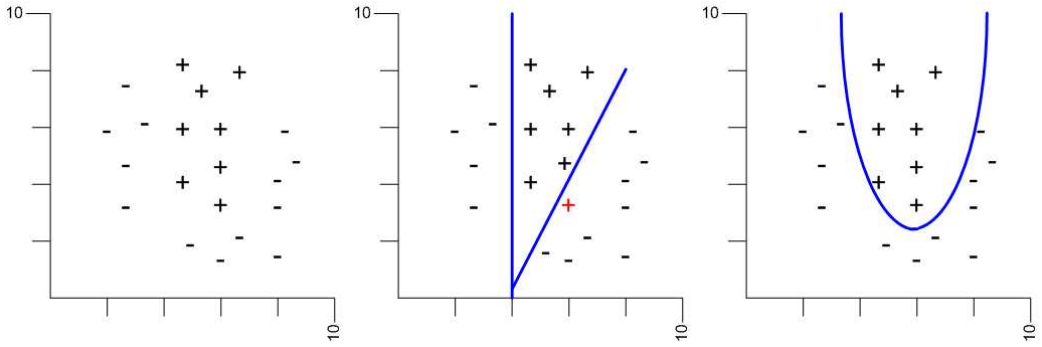

(a) Instance space

(b) Class separability using hypotheses consisting of lines

(c) Class separability using hypotheses consisting of parabolas

Fig. 2.9: Class separability problem

An example of overfitting is shown in Figure 2.10, where Figure 2.10 (a) shows the training instance space with the overfitting hypothesis drawn in black, that 'fits' the training data, but when tested with new data, the error rate increases (Figure 2.10 (b))

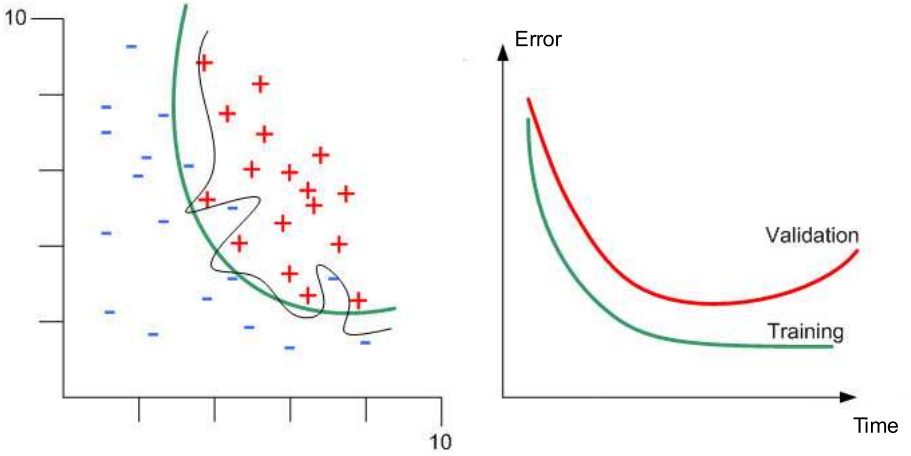

(a) Overfitting hypothesis

(b) Overfitting error curve

Fig. 2.10: Overfitting example

Jensen and Cohen [8] present several reasons for what overfitting is considered harmful:

1. Models with overfitting are incorrect since they inform a relationship with some variables when that relationship does not exist.
2. These models are more complex and thus require more space to store and more computational resources to process.
3. Irrelevant attributes require the collection of unnecessary data.
4. Models with overfitting are more difficult to understand.
5. The accuracy obtained with new test data is occasionally lower than the one obtained with training data.

2.2.2 *K-Means cluster analysis*

Cluster analysis is the process of grouping similar objects in the same class [16]. The similarity of two objects is determined by measuring the distance between them, which can be calculated in different ways, like Euclidean distance, normalized Euclidean distance, Mahalanobis distance, etc. [12].

The Euclidean distance e_{rs} between two points x_r and x_s is denoted by:

$$e_{rs} = \sqrt{(x_r - x_s)'(x_r - x_s)} \tag{2.8}$$

And the Mahalanobis distance m_{rs} between x_r and x_s is computed with the following equation:

$$m_{rs} = \sqrt{(x_r - x_s)'\Sigma^{-1}(x_r - x_s)} \tag{2.9}$$

being Σ an estimated variance-covariance matrix [12].

This thesis uses Euclidean distance. Cluster analysis belongs to the unsupervised learning group of algorithms, because the class of each individual is not known.

The clustering method used in this thesis is k-means. This algorithm requires to be indicated the number of clusters (k) to build, and performs an iterative process producing k groups of elements whose inter-cluster distance is minimum. The center of each cluster is called the *'center of mass'* and is the mean value of the elements of the cluster it belongs to [16].

The k-means algorithm can be described in these steps:

1. Randomly select k elements which will be used as the initial centers.
2. Assign each of the remaining elements to the cluster which similarity (distance) to the center is minimum.
3. Compute the new mean (center) of each cluster.
4. Repeat steps b) and c) until a stop criteria is met (i.e.: mean square error).

An example of k-Means clustering can be seen in Figure 2.11.

2.2.3 *Decision Trees*

Jan & Kamber [16] define a decision tree as a tree structure like a flow diagram, in which each node indicates a test on an attribute, each branch represents the result of that test and the leaf nodes represent classes.

Mitchell [36] argues that a decision tree is a method that is used to perform approximations when the objective functions are discrete. An advantage of the decision trees is

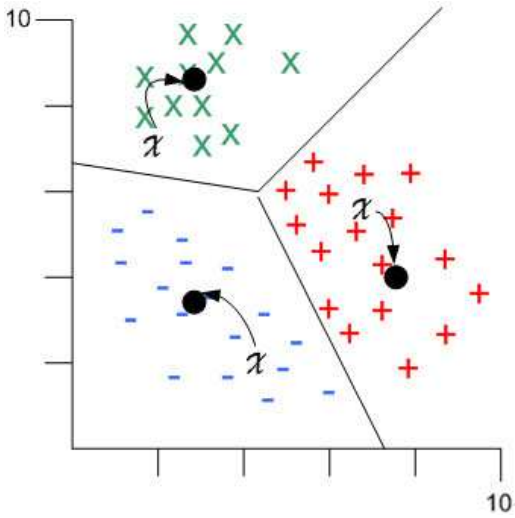

Fig. 2.11: K-Means clustering example: with each iteration, the center of each cluster is moved to the mean position of the group.

that they can represent the knowledge like IF-THEN rules, which are easy to interpret by humans.

As was previously mentioned, induction decision trees tend to suffer from overfitting, and one way to overcome this problem is by using pruning techniques [16].

Pruning methods use statistical measures to remove unnecessary branches in order to make the classification faster and improve the ability of classifying new data [16].

There exist two approaches to pruning:

1. **Pre-pruning:** Pruning occurs while the tree is being built by stopping the splitting of a node, and converting that node to a leaf [16]. A statistical measure and a threshold are used to determine when to stop splitting a node. If that threshold is high, it might build oversimplified trees, while low thresholds may result in overfitting [16].

2. **Post-pruning:** In this case, pruning takes place after the tree is fully built, by removing its branches according to a pruning algorithm which calculates the expected error rate of the tree if that branch is removed [16].

Next, we introduce the decision trees used in this research:

- **Iterative Dichotomiser 3 ($ID3$):** The $ID3$ algorithm, which was developed by Quinlan in 1986, is a supervised learning system which builds decision trees from a set of examples. Each example (instance) has a set of attributes and a class. The domain of the attributes and the class must be discrete. Furthermore, classes must be disjoint [36].

  To generate an initial decision tree from a training set, this algorithm uses the 'divide and conquer' strategy, because in each step this method performs a partition

of the data of the node according to a test performed over the most discriminative attribute [38].

The criteria used by $ID3$ to split the nodes is the Entropy. Entropy can be seen as the amount of information existing in the result of an experiment [44]. Thus, the $ID3$ algorithm chooses, for each decision node, the attribute with the highest discriminating capacity over the examples analyzed, which is the attribute that generates disjoint sets where the internal homogeneity is maximized (the variability minimized) with respect to the values of the class [44].

- **C4.5 and J48 decision Trees:** $C4.5$ was presented by Quinlan in 1993 as an extension of $ID3$ [38]. The splitting criteria used by this algorithm is the gain ratio. It also allows the possibility of performing a pessimistic post pruning of the resulting tree (substituting a subtree by a leave, or by one of its branches) [6]. The construction strategy is similar to $ID3$.

  The gain ratio criterion consists in building decision trees that use keys to make branches. It has been observed that this criterion tends to build unbalanced trees, a characteristic which inherits from the splitting rule that it derives (information gain). Both heuristics are based on an entropy measure which favors partitions of the training set unequal in size when one of them has all the instances belonging to the same class, despite only few instances of the training set belong to that partition [6].

  The J48 algorithm is a new version of Quinlan's $C4.5$ algorithm which is used in the data mining software WEKA. An example of a J48 tree is shown in Figure 2.12.

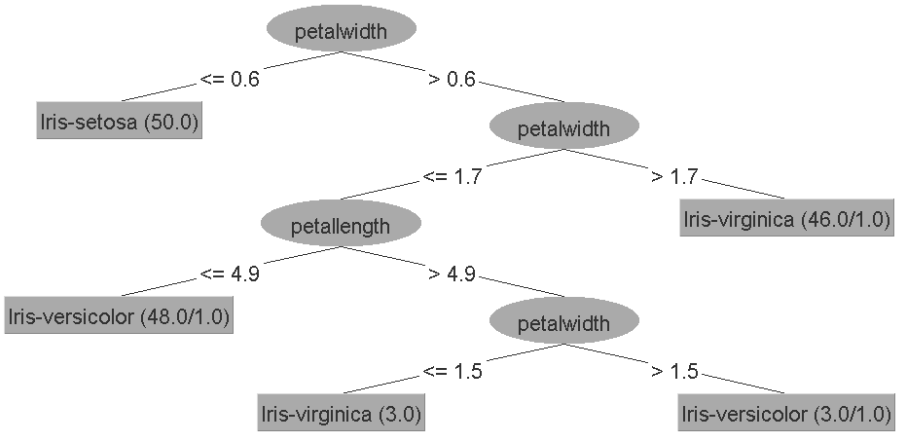

Fig. 2.12: J48 Decision tree for the Iris dataset

- **Classification And Regression Trees (CART):** Classification And Regression Trees is a method created by Breiman [31] that produces decision trees from categorical or continuous variables. If the variables are continuous, it makes a regression tree, and if they are categorical, it makes a classification tree. The splitting criteria used for classification are the Gini index, Chi-squared and G-squared; while the

splitting criteria used for regression is a least squared deviation criterion [31]. The trees obtained using this method are binary [6].

This algorithm also allows to perform a cost-complexity pruning with cross-validation [6].

- **Best First Tree:** Unlike traditional decision trees (i.e., C4.5, CART) which expand in depth, Best First trees expand selecting the node which maximizes the impurity reduction among all the available nodes to split. The impurity measure used by this algorithm is the Gini index and information gain [51].

- **Logistic Model Tree (LMT):** is a decision tree with the peculiarity that each leave is a logistic regression model [42]. While logistic regression only captures lineal patterns, decision trees generate non linear models. One of the disadvantages of this method is the increased computational complexity [42]. An example of a Logistic Model Tree which was generated in the calyx detection process is shown in Figure 2.13, where it can be seen that the leaves of the tree are logistic regressions.

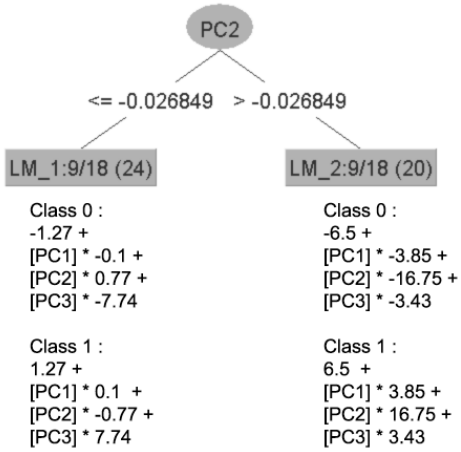

Fig. 2.13: Logistic Model Tree example for calyx detection

- **Random Forest:** generates a series of decision trees, where each tree is built using a vector generated randomly for each tree, but using the same distribution for all trees. After building a considerable amount of trees, each one votes for the most popular class, and the final model classifies with the class voted by the majority [30]. One interesting aspect of this classifier is that, given the law of large numbers, overfitting is not produced [30].

2.2.4 *Classification Rules*

- **One Rule (1R):** The One Rule (1R) algorithm makes a classification rule applying only a single attribute, producing a result similar to a single level decision tree [50]. This method makes very simple models and has been proved that with several data sets, it shows results as good as the ones achieved with more complex methods like C4.5 decision trees [50].

2.2.5 *Artificial Neural Networks (ANN)*

A neural network can be seen as a massively parallel distributed processor, made of simple processing units, which are capable of storing experimental knowledge and have it ready to be used later [52].

It resembles the human brain in which the knowledge is obtained from the environment through a learning process, and the neural interconnection strengths, known as synaptic weights, are used to store the acquired knowledge [52].

Biological brains are composed by neurons, which are cells that can process information. An example of a biological neuron is shown in figure 2.14 (a), where it can be seen that the structure of the cell consists of the cell body, the nucleus and a series of connectors named dendrites which are responsible for receiving the impulse from predecessor neurons. The axon transmits the impulse to the axon terminal branches where the synapses takes place transmitting the neuron's output to other neuron's dendrites through a chemical process [52].

The artificial counterpart, which diagram is shown in Figure 2.14 (b), has a series of input signals (equivalent to dendrites), synaptic weights (equivalent to the synapses), an activation function (equivalent to the cell body) and the output of the neuron [19].

The mathematical formula of an artificial neuron is denoted by:

$$y_k = \varphi(\sum_{j=1}^{n} w_{kj}x_j + b_k) \tag{2.10}$$

where $w_{k1}..w_{k1n}$ are the synaptic weights, $x_1..x_n$ are the input signals, b_k is the bias, $\varphi(.)$ is the activation function and y_k is the output signal. The bias b_k is used to move the threshold of the activation function [52].

The activation function $\varphi(.) : \mathbb{R} \rightarrow \mathbb{R}$ has the effect of limiting the amplitude of the output of the neuron. Examples of activation functions are shown in Figure 2.15.

Artificial Neural Networks are useful in pattern recognition applications, such as visual inspection systems, where the human brain outperforms computer systems. For example, [36] mentions that although human brains switching speed is about 10^{-3} seconds while computer's switching speed is in the order of 10^{-10} seconds, it takes only 10^{-1} seconds for a human to visually recognize his mother. This

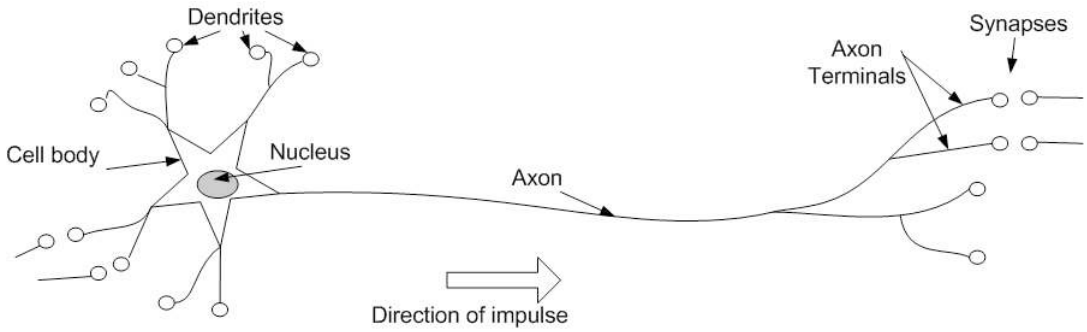

(a) Biological neuron structure

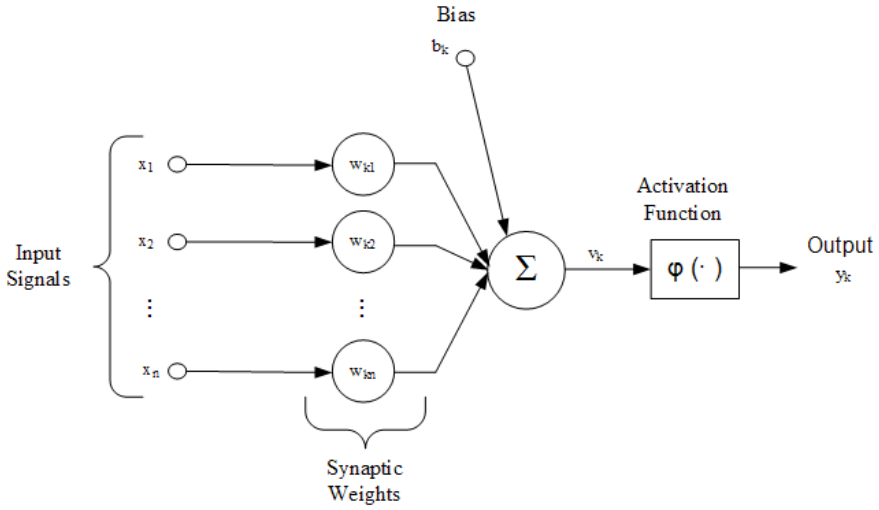

(b) Artificial neuron diagram

Fig. 2.14: Biological and Artificial neurons

behaviour is thought to be achieved by the distributed representation and highly parallel processing of the human brain, and this is the motivation of artificial neural networks architecture [36].

However, there exist several differences between Artificial Neural Networks and biological brains, like the hormones flow that is not modeled in ANNs, or the fact that ANN output a single constant value while biological neurons output a series of complex time series of spikes [36].

- **Multilayer Perceptron Neural Network with Backpropagation (MLP):** The 'Multilayer Perceptron' neural network has an input layer made of input nodes or 'sensory units', one or many hidden layers and an output layer. During the training step, the input signal spreads forward from the input layer to the output layer, producing a result. This result is compared to the desired value and errors are calculated in the opposite direction while the synaptic weights are adjusted. Due to this error propagation process from the output layer to the input layer, this algorithm is known as 'Backpropagation'

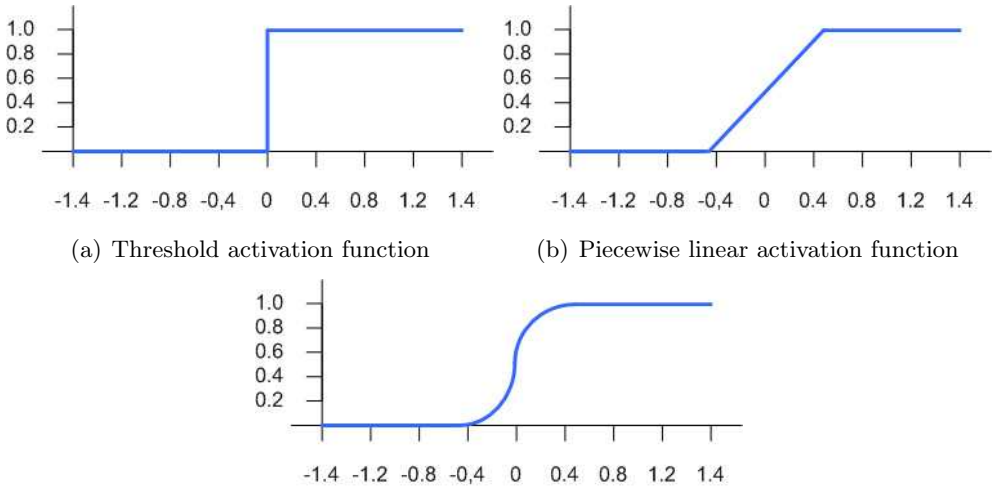

(a) Threshold activation function

(b) Piecewise linear activation function

(c) Sigmoid activation function

Fig. 2.15: Activation functions

- **Radial Basis Function Network (RBF Network):** Unlike the multilayer perceptron with backpropagation algorithm which uses a recursive approximation technique known as stochastic approximation, the RBF network can be seen as a curve fitting problem in a high dimension space, where it has to find the best surface to fit the training data [52]. The network has three layers. The first layer is the input from the outside, the second is a hidden layer that makes a non linear transformation from the input space to the high dimension hidden space. The third layer is the output layer and shows the response of the neural network to the input data [52].

- **Sequential Minimal Optimization for Support Vector Machines (SMO):** Support Vector Machines are linear classifiers that learn in a batch mode basis. The learned classifier consists of an hyperplane, and the classification is performed by computing the sign of the dot product of the data point with the classifier [53]. During the training of a support vector machine, it is required to find the solution to a large quadratic programming (QP) problem. The SMO algorithm divides this problem into many smaller QP problems, and they are solved analytically requiring fewer computational cost [47].

2.2.6 ***Attribute selection methods***

Despite most data mining algorithms are capable of getting rid of non discriminant attributes, in many cases better results are obtained if the dataset is previously processed with attribute subset selection algorithms. Furthermore, algorithms often get their speed reduced by irrelevant or redundant data, which can be discarded in an early stage by applying attribute selection methods before training the main machine learning algorithm [40].

In the following paragraphs, we briefly explain each of the attribute selection methods used in this thesis.

- **Correlation based feature subset selection (CFSSubset):** This method consists in the evaluation of the worth of a subset of attributes taking into consideration the individual predictive power of each attribute and the degree of redundancy between them [40]. By removing irrelevant attributes, the hypothesis search space is reduced, and in some algorithms, the required storage gets also reduced. Hall and Smith describe the hypothesis in which the heuristic is based as: 'Good feature subsets contains features highly correlated with the class, yet uncorrelated with each other' [40].
- **Information Gain attribute evaluation:** This method uses information theory to measure the information gain of each attribute in order to determine the discriminant level of each attribute with respect to the class. [18].
- **Chi Squared Attribute Evaluator for features subset selection:** This method uses the Chi Squared statistic to evaluate the importance of each attribute with respect to the class [18].

2.2.7 Classifier performance evaluation

In classification problems with only two classes, each instance I of the data set is evaluated an mapped to one of the classes: p (positive) or n (negative) [55]. The result of the classification can be either correct or wrong, so there are four possibilities:

1. TP: A true positive is when a positive instance is correctly classified as positive
2. TN: A true negative is when a negative instance is correctly classified as negative
3. FP: A false positive is when a negative instance is wrongly classified as positive
4. FN: A false negative is when a positive instance is wrongly classified as negative

The combination of these values are presented in a matrix form, known as the **Confusion Matrix**, like the one shown in Table 2.1

Predicted class / True class	Positive	Negative
Positive	TP	FN
Negative	FP	TN

Tab. 2.1: Confusion matrix example

Classifier performance can be evaluated by different metrics:

- **Accuracy:** $\frac{TP+TN}{TP+TN+FP+FN}$
- **Precision:** $\frac{TP}{TP+FP}$
- **False positive rate** (hit rate): $\frac{FP}{FP+TN}$
- **True positive rate=Recall:** $\frac{TP}{FN+TP}$
- **F-measure**: $\frac{2}{1/precision+1/recall}$
- **Error rate** $1 - accuracy$

As predictive accuracy has been widely used as the main evaluation criterion [32], we use this metric to compare classifier performance.

However, there exist better ways to measure the performance of a classifier. The area under the ROC (receiver operating characteristics) curve (AUC) is considered by many authors a much better metric than accuracy for evaluating learning algorithms [32].

One of the reasons why classification accuracy is not always suitable resides in the fact that accuracy assumes equal misclassification costs, and most of the real time problems fail in this assumption [15]. Furthermore, accuracy maximization assumes that class priors are known for the target environment [15].

The AUC metric not only overcomes these drawbacks, it also has increased sensitivity in ANOVA tests and is independent to the decision threshold [32]. ROC curves have also the advantage that describe the predictive behavior of the classifier independent of class distribution or error costs [15].

We use the AUC metric to compare classifiers performance when predicting two class problems (calyx detection and orange quality classification in two classes).

An example of a ROC curve is shown in Figure 2.16, where it can be seen that a ROC plot has two axis: The true positive rate TP is drawn in the Y axis, and the false positive rate FP is drawn in the X axis. Note that a confusion matrix corresponds to one point in the ROC curve [55].

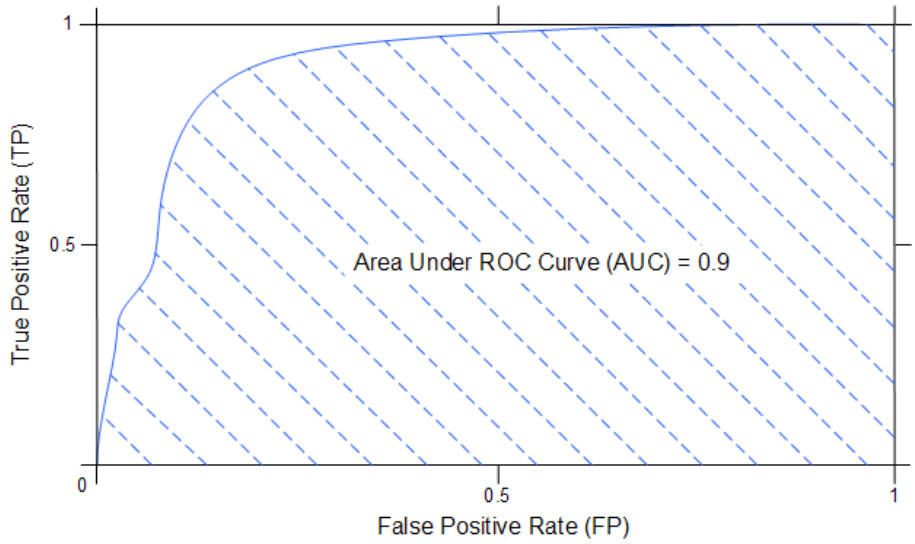

Fig. 2.16: Receiver Operating Characteristics (ROC) curve example for calyx detection

2.3 ***Conclusions***

Data mining and Digital image processing are both useful tools that can be used together to perform several tasks like automated visual inspection.

Digital image processing is the set of methods used to process images in the digital domain, like color space conversions, shape and texture analysis, image segmentation, etc. In this section we explained how a digital image is represented in a computer, which are the different ways to represent and process color images, and we also explained several morphological operations performed over binary images. In this thesis we use image processing techniques to compute features from digital images which are then used by the data mining algorithms to perform the classification.

We also introduced Machine learning and Data mining concepts, as well as a brief description of all the steps in the Knowledge discovery in databases process. We focused on classification algorithms like decision trees and neural networks since these group of algorithms are the ones used in the classification step. We also analyzed the different metrics used for analyzing classifiers performance, choosing the accuracy and the area under the ROC curve (AUC) as the most suitable indicators to compare classifiers performance in this thesis.

3. SYSTEM OVERVIEW

The whole orange quality grading system consists of four subsystems. The first one captures the orange picture, the second one detects and removes the calyx area, the third one performs the classification into different quality categories, and the last one places the fruit already classified in the desired container.

This thesis focuses on the calyx detection and classification subsystems, which are explained in detail in chapters 4 and 5.

The operation of the system is described as follows: Oranges move in the conveyor belt and enter one by one in the inspection chamber, where a camera with a set of mirrors capture the images from different angles, except the bottom view which is blocked by the conveyor belt.

Then, the calyx detection system detects defects and the calyx. In order to avoid confusions, the calyx is removed from the image. This step is very difficult because the calyx can be confused with a defect. Finally, the resulting images are processed and oranges are classified.

A diagram of this mechanism is shown in Figure 3.1

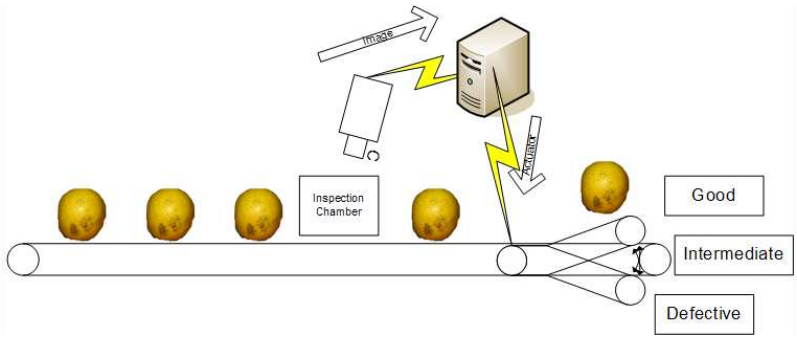

Fig. 3.1: Diagram of the system where oranges images are captured, analyzed and classified into three categories

3.1 *Image capture*

The image capture system consists of a conveyor belt and an inspection chamber where images are captured by a digital camera. The main difficulty of capturing the image is to be able to capture the picture from all angles, without loosing any section of the orange's skin.

There exist many alternatives for solving the problem of not being able to capture the bottom view.

One solution to solve this inconvenient is the one proposed by Recce et al. [37]. They suggest that the fruit travel over a conveyor belt at a known constant speed, which throws the fruit in the air to perform the capture from all possible angles. This method is illustrated in Figure 3.2 (a).

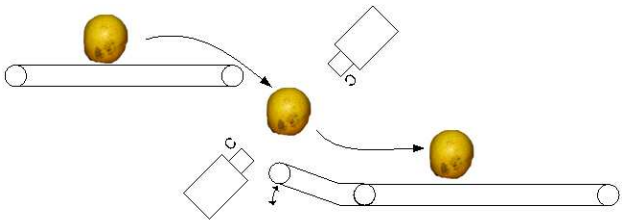

(a) The fruit is thrown in the air while a camera captures the images from all possible angles

(b) Peeling

(c) Mirrors

Fig. 3.2: Different approaches of capturing images from different angles.

The disadvantage of this solution is the increased complexity to synchronize the shooting time to capture the image, with the position of the orange in the air.

Another solution is the one proposed by D'Amato et. al where they 'virtually peel' an apple by using a video camera which captures between 3 and 5 images of the same fruit while it is being rotated by the cilindres of the conveyor belt [45]. By doing this, each image contains a picture of the fruit from different angles. Finally, all images are put together (removing redundant data) and that image is the one used for processing.

A sample image is shown in Figure 3.2 (b). A similar approach is employed by [46] but using more images of the same fruit to perform a cylindrical projection approximation.

A third approach employed in [28] consists in using several mirrors to capture images from different angles, as if multiple cameras were used. One of the disadvantages we find in this approach is that, depending on where the defect is located, it may appear reflected in more than one mirror, increasing the chances of downgrading that specimen.

In our experiment, we capture the images manually using a digital camera and using three mirrors to obtain images from different angles.

3.2 ***Classified oranges placement***

Once a fruit is classified, the system has to take an action according to the obtained results. The machine consists of a series of gates placed at the end of the conveyor belt to divert the fruit according to the classified quality level, and deposit it in the desired container.

3.3 ***Conclusions***

Along this chapter we showed an overview of the orange grading system, and we explained the image capture and classified oranges placement subsystems, which are the subsystems that are not part of the main topic of this thesis. We have discussed the inconvenients faced when acquiring the image and the advantages and disadvantages of the solutions proposed by different authors found in the literature. After analyzing the different approaches for capturing the images, we chose the mirror approach because of the efficiency of its implementation.

4. CALYX DETECTION

The calyx or stem-end of an orange fruit is the section where the stem attaches the fruit. It has a circular and symmetrical shape, and it often presents radial lines that radiate from the calyx area.

As part of an automatic fruit grading system, the detection of the stem-end/calyx is a major task required in order not to misclassify calyxes as defects. An accurate calyx detection will therefore improve the overall accuracy of the fruit grading system.

For the purpose of this work, we consider stem-ends and calyxes as synonyms.

The calyx detection sub-system is further divided into the following steps:

- Pre-processing
- Segmentation
- Feature extraction
- Classification

A diagram of this process is shown in Figure 4.1.

The outcome of the calyx detection system is shown in Figure 4.2.

4.1 ***Pre-processing***

Pre-processing consists in improving image quality as noise reduction or contrast and brightness enhancement [9]. The goal of the pre-processing step is to improve the precision and speed of feature extraction algorithms. An example of pre-processing can be seen in Figure 4.3 where the original image is sharpened, its contrast and brightness are enhanced and its size is reduced.

4.2 ***Segmentation***

Segmentation consists of splitting up the image in regions in order to extract the objects of interest [9, 49]. In the pre-processing step we improve the contrast of the image, and in the segmentation step we remove the background and extract candidate regions where it is likely to find a calyx/stem-end.

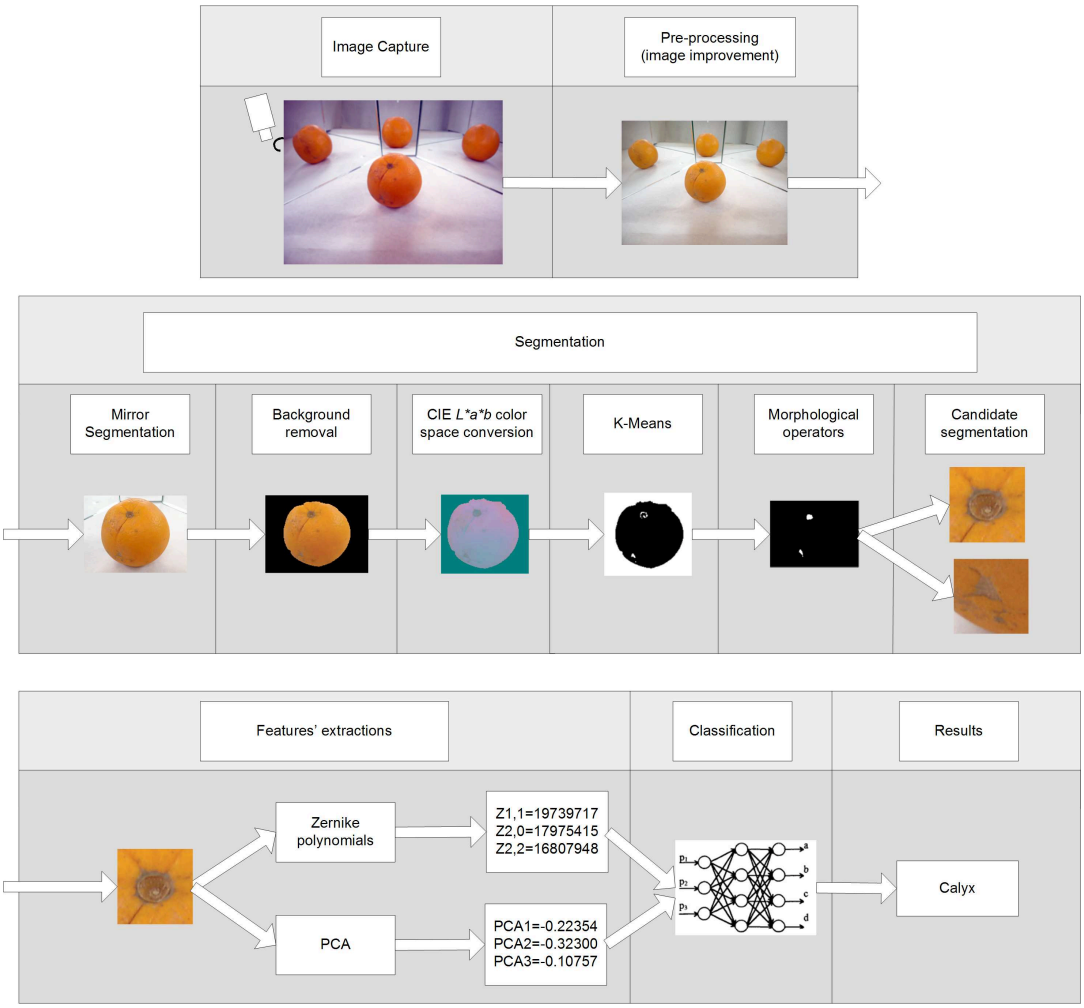

Fig. 4.1: Image processing steps for calyx/defect classification: The oranges images are captured, segmented into subimages of calyx or defect candidates, features are extracted, and the image is classified as calyx or defect.

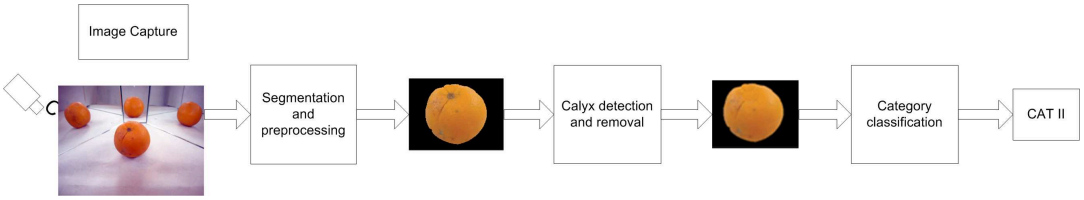

Fig. 4.2: Example of the calyx detection system where an image is analyzed, its calyx is detected and removed, and the orange is classified.

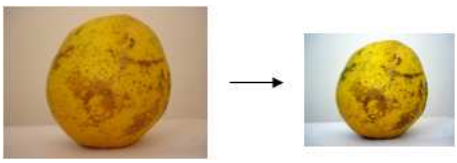

Fig. 4.3: Pre-processing example: The original image is sharpened, its contrast and brightness are enhanced and its size is reduced

Background removal: Being I_o and I_b the regions for the orange (foreground) and background, we extract the region I_o from the background by first improving the contrast of the image I and extracting the blue component from the RGB color space.

The choice of the blue component is because it is the component that most discriminates the background of the image, due to the fact that for the orange color (made of red and some green), the value of the blue component is zero. This can be seen in Figure 4.4.

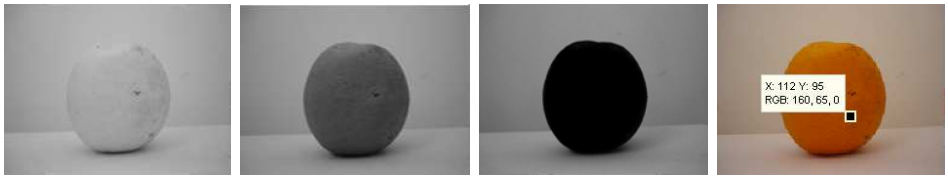

(a) Component R (b) Component G (c) Component B (d) RGB with 1 pixel

Fig. 4.4: Red, Green and Blue (RGB) components of an image.

The gray-level image obtained is then converted to black and white followed by morphological operations (erosion and dilation) for noise reduction [49]. After obtaining a binary image, a contour tracking algorithm is used to detect the border of the orange in the original color image to extract the background [49].

This process is done for every image captured.

Mirror segmentation: When using mirrors in the capture step, it is necessary to identify the different sections of the image where an orange is found. The process is similar to the background removal: first we improve the contrast of the image and extract the blue component. Next, the image is binarized, morphological operators are applied following by a contour tracking algorithm. An example of the original image with the contours of the orange highlighted is shown in Figure 4.5.

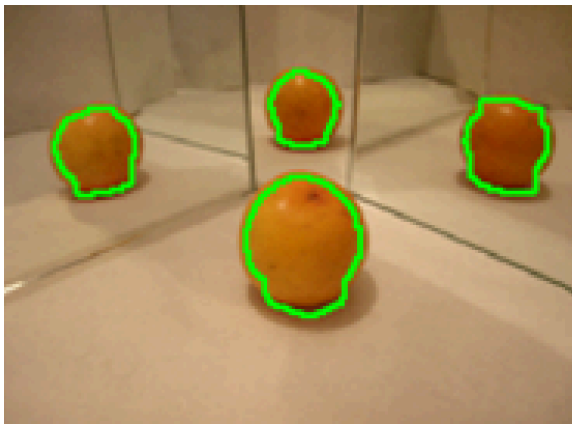

Fig. 4.5: Mirror segmentation

Calyx candidate regions extraction:

- **CIE L*a*b* Color space conversion:** The first step is to convert the image with the background removed to the CIE L*a*b* color space. As it was previously explained in section 2.1.2, the CIE L*a*b* color space is considered as one of the best color spaces for matching the human perception distance of colors [14]. This is because the difference between two colors can be related to the perceptual distance [14] and thus it is a useful color space to perform cluster analysis. The color space consists of three layers. The Luminance or brightness layer $L*$, the Red-Green chromatic layer $a*$ and the Blue-Yellow chromatic layer $b*$ [26].

  Once the color space conversion is done, we discard the $L*$ component (because it does not contain color information), and perform a non supervised cluster analysis to detect different regions.

- **K-Means cluster analysis:** Cluster analysis is the process of grouping similar objects into the same class [16]. The similarity of two objects is determined by measuring the distance between them, which can be calculated in different ways, like Euclidean distance, normalized Euclidean distance, Mahalanobis distance, etc. [12].

  In this thesis we use k-means clustering with Euclidean distance and the number of clusters chosen is k=2, aiming to find two regions: one for the healthy skin and other for the calyx or defect. The distinction between calyxes and defects is performed in a further step.

The result of the k-means process is a binary image with two regions: The region of healthy skin and the region of the calyx or defect. However, as the image obtained can be noisy, morphological operators are applied. A scheme of this process is shown in Figure 4.6. It is performed for every image captured obtaining a total of n_c calyx candidate images.

As the aim of this process is to identify the region where a calyx could be found, and we know the average diameter of the calyx in an image, we discard the candidate regions which have a diameter smaller than the average (about 5 pixels in 192x144 pixel images).

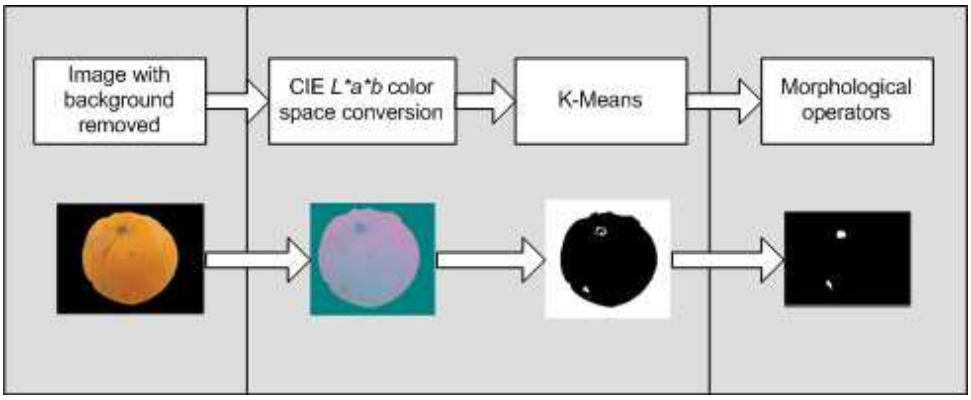

Fig. 4.6: K-Means clustering after performing CIE L*a*b* colorspace conversion

4.3 ***Feature extraction***

Once the image is segmented, it is necessary to obtain several features in order to be able to perform the classification.

The objects in the image can be characterized by different descriptors like gray levels, color, texture, gradient, second derivative and by geometrical properties like area, perimeter, Fourier descriptors and invariant moments [43, 9]. For instance, Unay & Gosselin [10] extract the background, stem, good peel and defective peel for classifying oranges.

In this section, the features obtained are a series of Zernike moments and the first ten Principal Components.

We choose Zernike moments for calyx detection because they are rotation invariant [1], which makes them suitable for analyzing symmetrical objects like calyxes. Zernike moments are very useful in image processing and recognition, and are widely used in face detection applications, like in [29], where authors perform eye detection using Zernike Moments and use a Support Vector Machine for classification.

In [5], a face recognition system for video surveillance is presented, where they perform a comparison between Zernike moments, Eigenfaces (Principal Component Analysis) and Fisherfaces.

Other image processing applications which use Zernike polynomials include a system presented by [39] which uses Zernike polynomials to model the global shape of the cornea, and use a decision tree classifier which takes as features the polynomial coefficients.

Other reason for trying Zernike polynomials are the good results obtained by Recce et. al [37] for stem-end/calyx detection in oranges. We also choose to use Principal Component Analysis as they are widely used in image processing tasks like face recognition (eigenfaces) [7], and also for stem end/calyx detection in apples [20].

4.3.1 *Zernike Moments*

Zernike Moments moments are very useful in image processing and recognition because they are rotation invariant and form a complete orthogonal set over the interior of the unitary circle [1]. The projection of the image over these sets are the Zernike moments [2]. The form of the polynomials is denoted by

$$Z_{nm}(x,y) = Z_{nm}(\rho,\sigma) = R_{nm}(\rho)e^{(jm\theta)}, \tag{4.1}$$

where $j = \sqrt{-1}$, ρ is the length from origin $(0,0)$ to (x,y), and θ the angle between the x axis and the vector from origin to (x,y) in a counter clockwise direction, $n \in N_0$ is the order of the polynomial, and $m \in Z$ is the rotation degree [3].

The restriction: $n - |m|$ is even and $|m| < n$ [1] has to be satisfied.

$R_{nm}(\rho)$ is the radial polynomial defined by

$$R_{nm}(\rho) = \sum_{s=0}^{(n-|m|)/2} \frac{(-1)^s (n-s)! \rho^{n-2s}}{s!(\frac{n+|m|}{2}-s)!(\frac{n-|m|}{2}-s)!} \tag{4.2}$$

and according to Euler's formula: $e^{(jm\theta)} = cos(m\theta) + jsin(m\theta)$.

The Zernike moment A_{mn} for a continuous function $f(x,y)$ is defined as

$$A_{nm} = \frac{n+1}{\pi} \int\int_{x^2+y^2 \leq 1} f(x,y) Z^*_{nm}(\rho,\theta) dxdy \tag{4.3}$$

and for a digital image of size $M \times N$ as

$$A_{nm} = \frac{n+1}{\pi} \sum_{x=1}^{M} \sum_{y=1}^{N} f(x,y) Z^*_{nm}(\rho,\theta) \tag{4.4}$$

where [*] denotes the complex conjugate [4]. A_{nm} can also be seen as the multiplication of the original image $f(x,y)$ with a mask. Each component of the image A_{nm} is a complex value. In Figure 4.7 an image of a Zernike mask of order $Z_{5,1}$ is shown.

For every image from the previous step, we compute the Zernike moments from order n=1 to order n=12, so we obtain 48 Zernike-images. The first 12 Zernike Moments and their dimensions are shown in Table 4.1. For each one we calculate the sum of the absolute values of each pixel and these values are used in the classification step.

(a) $Z_{5,1}$ Real

(b) $Z_{5,1}$ Imaginary

Fig. 4.7: Zernike moment masks examples for n=5, m=1

Order n	Dimension	Zernike Moments
0	1	$Z_{0,0}$
1	2	$Z_{1,1}$
2	4	$Z_{2,0}$ $Z_{2,2}$
3	6	$Z_{3,1}$ $Z_{3,3}$
4	9	$Z_{4,0}$ $Z_{4,2}$ $Z_{4,4}$
5	12	$Z_{5,1}$ $Z_{5,3}$ $Z_{5,5}$
6	16	$Z_{6,0}$ $Z_{6,2}$ $Z_{6,4}$ $Z_{6,6}$
7	20	$Z_{7,1}$ $Z_{7,3}$ $Z_{7,5}$ $Z_{7,7}$
8	25	$Z_{8,0}$ $Z_{8,2}$ $Z_{8,4}$ $Z_{8,6}$ $Z_{8,8}$
9	20	$Z_{9,1}$ $Z_{9,3}$ $Z_{9,5}$ $Z_{9,7}$ $Z_{9,9}$
10	26	$Z_{10,0}$ $Z_{10,2}$ $Z_{10,4}$ $Z_{10,6}$ $Z_{10,8}$ $Z_{10,10}$
11	42	$Z_{11,1}$ $Z_{11,3}$ $Z_{11,5}$ $Z_{11,7}$ $Z_{11,9}$ $Z_{11,11}$
12	49	$Z_{12,0}$ $Z_{12,2}$ $Z_{12,4}$ $Z_{12,6}$ $Z_{12,8}$ $Z_{12,10}$ $Z_{12,12}$

Tab. 4.1: First 12 Zernike Moments

4.3.2 ***Principal Component Analysis (PCA)***

PCA is a procedure used in multivariate data analysis which performs an orthogonal linear transformation to a set of correlated variables into a set of non correlated variables called principal components (PC) [12]. One of the main purposes of this procedure is to obtain a dimensionality reduction. Principal Component Analysis is used in several applications in image processing, specially with large datasets or very large images like satellite images.

The projection of the variables into the new coordinate system is also called the Karhunen-Loéve transform (KLT) or Hotelling transform [7].

When this method is applied to a set of correlated variables in a space of dimension D, the transformation diagonalizes the covariance matrix and creates a new coordinate

system. These coordinates are the Principal Components and they are sorted by decreasing variance. This means that low order components explain the highest variance of the data, and by keeping the P first components, most of the variability is retained, leading to a dimensionality reduction ($P << D$) [12, 7].

The criterion used in this thesis for deciding how many components P are enough to explain most of the variance, are the following:

1. The first criterion consists of adding the explained variance for each Principal Component until the accumulated explained variance is higher than a certain threshold (e.g. 80% of the total variance) [12]. Figure 4.8 (a) shows an example of this plot.

2. The second criterion is based on a SCREE plot of eigenvalues. The point in which the curve tends to stabilize is the number of components required. An example is shown in Figure 4.8 (b). In this example, the number of components to be chosen should be five, since in that component the curve tends to stabilize.

3. The third criterion, which is valid only for PCA analysis using the correlation matrix, consists of keeping the eigenvalues greater than 1, so the dimension of the space is equal to the number of eigenvalues greater than 1.

The first two criteria can be applied when using both the variance-covariance matrix and the correlation matrix, and the third can only be applied when using the correlation matrix [12].

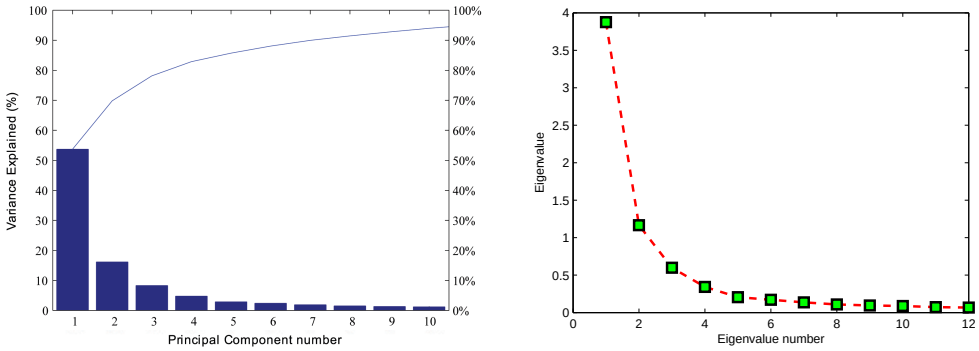

(a) Pareto plot which shows the percentage of variance explained.

(b) SCREE plot.

Fig. 4.8: PCA evaluation criteria.

In this thesis, we perform the Principal Components Analysis in the following way: for every calyx candidate image I_{cc} of size $M \times N$ obtained in the segmentation step, we first convert from RGB to HSV to obtain the hue component and then convert the image matrix to a vector of size $1 \times M \times N$, obtaining a dataset of size $n_c \times M \times N$ of real values ranging from 0 to 1, being n_c the number of calyx candidate images of the dataset.

The choice of the H component was done empirically comparing the results of performing PCA using R, G, B, H, S, V, and gray level components. These results are shown in Figures 4.9 (a) and (b), where it can be seen that while the variance explained by the first principal component is higher when using the Red and Saturation components compared to the variance explained by the first component of the Hue component, the eigenvalues of the second and third principal components of H are much higher than in the others, thus the accumulated variance explained of H is higher than in the rest.

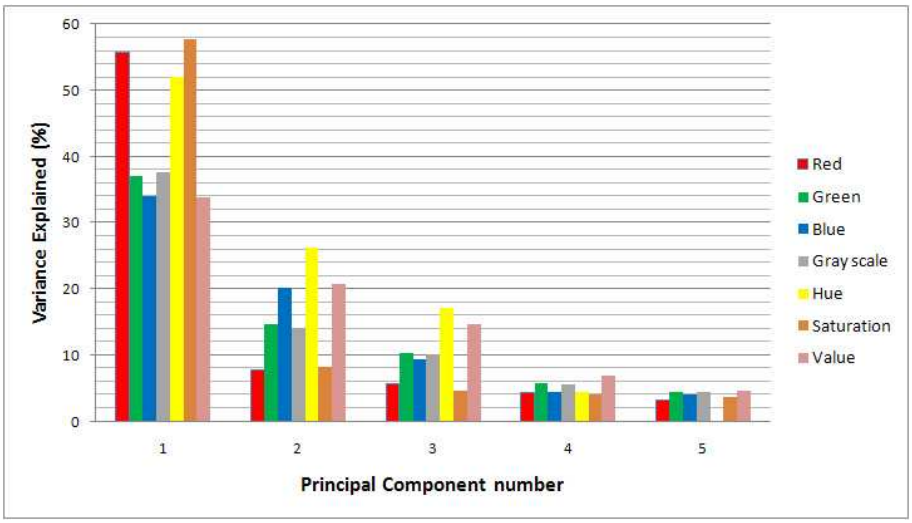

(a) SCREE plot

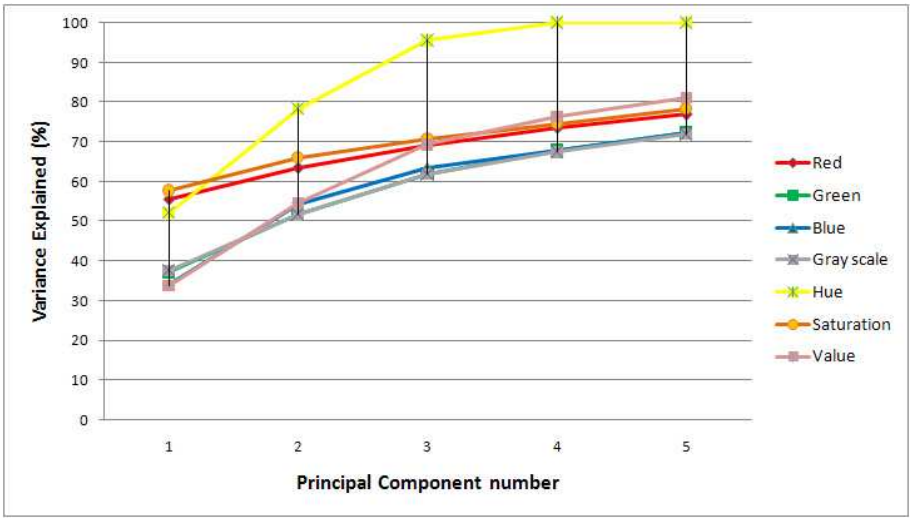

(b) Accumulated SCREE plot

Fig. 4.9: SCREE plots showing the variance explained by performing PCA over each component of the RGB and HSV color spaces

As all the variables are in the same unit and within the same range, we perform the Principal Component Analysis over the covariance matrix, without needing to standardize the data [12]. The results of the PCA are the coefficients of the linear transformation (C_{pca}), which are used to obtain the projected images (P_{ij}) in the new coordinate system.

In [12], the number of components P needed in the classification step is P=3 or P=4. If we consider the SCREE plot, the number of components when the curve stabilizes is around P=5. However, in order to compare the performance of the classifiers using many different number of PCs, we keep the first ten principal components to use them in the classification step.

An example of the values of the first two components for classifying calyxes or defects is shown as a scatter plot in Figure 4.10.

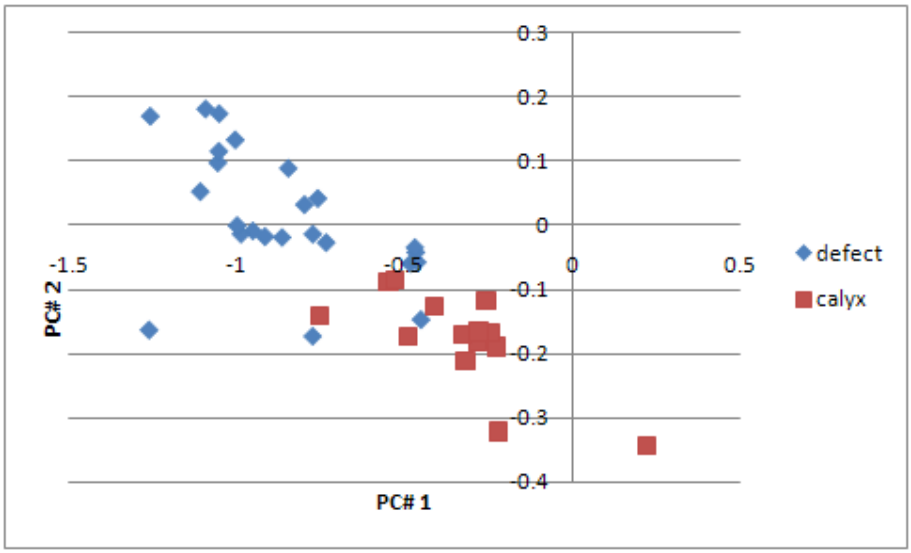

Fig. 4.10: Scatter plot of the first two principal components for calyx and defect detection

Once the features of the Zernike moments and Principal Components are extracted, a consolidated dataset is built. It contains n_c rows (one for each calyx candidate), and 58 columns (48 from the Zernike moments and 10 from the first PCs). Also the class was added to the dataset in order to use supervised learning algorithms.

4.4 Classification Results

4.4.1 Validation methods

Once a classification model is built using training examples, the model is validated with unknown instances. For this purpose, we use ten fold cross validation to validate the algorithms. This consists of partitioning the data set in k subsets, using $k-1$ subsets for training and model generation, and the other subset to validate the obtained model. This process is repeated k times using always a different subset for the validation, and finally all the results are averaged to produce a single estimation [48].

After applying different models, we analyze the confusion matrix, Area under the ROC curve (AUC) and compare the accuracy of the classifiers (percentage of cases correctly classified over the total of cases classified).

4.4.2 Datasets

For the calyx detection experiment, we use a total of 861 pictures, where in 234 images the calyx is visible, and in 627 images the calyx is hidden.

During the pre processing and segmentation steps, from the 234 images where there is a calyx, 221 candidate regions with a calyx are obtained, which means that 94.44% of the calyxes are found. The ones not detected are mostly because the calyx is near the border of the orange. This is not a big issue since the calyx not detected in one image is detected in other image of the same orange but taken from a different angle when using the mirror system.

We also obtain 85 candidate regions where there is not a calyx present (there's a defect), leading to a total of 306 calyx candidate pictures in which 72.22% are possitive examples, so the accuracy classification baseline is 72.22%. This means that a random classifier obtains a 72.22% accuracy, so data mining algorithms should improve this value.

The features extracted are the 48 Zernike moments and the 10 first Principal Components

Calyx classification results are shown in Table 4.3 and Figure 4.11.

4.4.3 Calyx Classification Results

Using Zernike Moments:

When using all the 48 Zernike moments, the best results are obtained by the Logistic Model Tree (LMT) with 88.22% accuracy and an Area under the ROC curve (AUC) of 0.89, followed by the Multilayer Perceptron neural network with Backpropagation (MLP) algorithm a 87.9% accuracy and an AUC of 0.9.

However, when using only the first 5 moments, the Multilayer perceptron increases its accuracy to 88.88% and AUC to 0.91, and the Logistic model tree achieves 88.66% accuracy with an AUC of 0.91.

Also, good results are obtained when using only the first 3 Zernike moments: the Multilayer perceptron achieves an accuracy of 88.87% and an AUC of 0.91 while the Logistic Model Tree has an accuracy of 88.12% and an AUC of 0.91.

We perform Chi Squared Attribute Evaluation with Ranker, and pick-up the first 20 attributes to perform the classifier's comparison. The results obtained are worse than using all the 48 Zernike moments: MLP and LMT achieve an accuracy near 84% and an AUC near 0.9, while SMO and RBF Network equal the baseline accuracy of 72.24%.

Using Principal Component Analysis (PCA): The best accuracy is obtained when using only the first 10 principal components, and is achieved by the Radial Basis Function Network with 81.05% accuracy and an AUC of 0.84. The same algorithm obtains an accuracy of 80.82% and an AUC of 0.86 when using only the first three principal components.

Combining Zernike Moments and Principal Component Analysis: We perform several combinations of Zernike moments and principal components. The best results are obtained with the Logistic Model tree when combining the first 5 Zernike moments with the first two principal components, obtaining an accuracy of 89.87% and an AUC of 0.93.

We also obtained similar results with the Multilayer Perceptron Neural Network when combing the first 5 Zernike moments with the first principal component, achieving an accuracy of 88.89% and an AUC of 0.92.

The confusion matrix of these classifiers are shown in Table 4.2

Algorithm	Predicted class / True class	Calyx	Defect	Accuracy	AUC
Zernike 5, PCA 2 LMT	Calyx	213	8	89.87%	0.93
	Defect	23	62		
Zernike 5, PCA 1 MLP	Calyx	209	12	88.89%	0.92
	Defect	22	63		

Tab. 4.2: Calyx classification confusion matrices

Attributes	RBF		SMO		MLP		LMT	
	%Accu.	AUC	%Accu.	AUC	%Accu.	AUC	%Accu.	AUC
Zernike48	72.24	0.60	74.63	0.55	87.90	0.90	88.22	0.89
Zernike10	72.24	0.61	72.24	0.50	88.66	0.91	88.10	0.90
Zernike5	72.24	0.63	72.24	0.50	**88.88**	**0.91**	**88.66**	**0.91**
Zernike4	72.24	0.63	72.24	0.50	88.77	0.91	87.79	0.90
Zernike3	72.34	0.63	72.24	0.50	88.87	0.91	88.12	0.91
PCA 10	**81.05**	**0.84**	72.89	0.52	76.60	0.74	77.35	0.73
PCA 5	80.06	0.86	73.33	0.52	78.12	0.77	79.41	0.82
PCA 3	**80.82**	**0.86**	72.68	0.51	78.33	0.77	77.78	0.82
PCA 2	80.29	0.86	72.24	0.50	78.87	0.79	78.46	0.83
PCA 1	77.35	0.76	52.24	0.50	75.28	0.40	75.61	0.68
Zer48, PCA10	73.53	0.75	78.66	0.63	87.38	0.85	88.97	0.85
Zer10, PCA10	80.73	0.78	74.33	0.53	86.83	0.84	87.44	0.84
Zer5, PCA10	81.27	0.80	73.22	0.53	86.61	0.83	87.23	0.83
Zer5, PCA2	78.51	0.78	72.78	0.51	87.79	0.91	**89.87**	**0.93**
Zer5, PCA1	73.52	0.73	72.24	0.50	**88.89**	**0.92**	87.79	0.91
Zer ChiSq.20	72.24	0.63	72.24	0.50	83.98	0.90	83.86	0.89
Zer ChiSq.5	71.80	0.64	72.24	0.50	71.14	0.64	71.69	0.50

Tab. 4.3: Calyx classification results

4.5 ***Calyx removal***

Once the classification result of a candidate region is obtained, we take different actions depending if the result is a calyx or a defect. On the one hand, if the candidate region is classified as a calyx, we replace in the original image of the orange, the section detected as a candidate region with the mean color of the rest of the orange. Doing this, the calyx is replaced by the mean color of the orange's skin so the orange grading subsystem will not mistake a calyx as a defect.

On the other hand, if the candidate region is classified as a defect, we add 1 to the defects counter of the orange being analyzed, which will be used as a feature in the orange classification step.

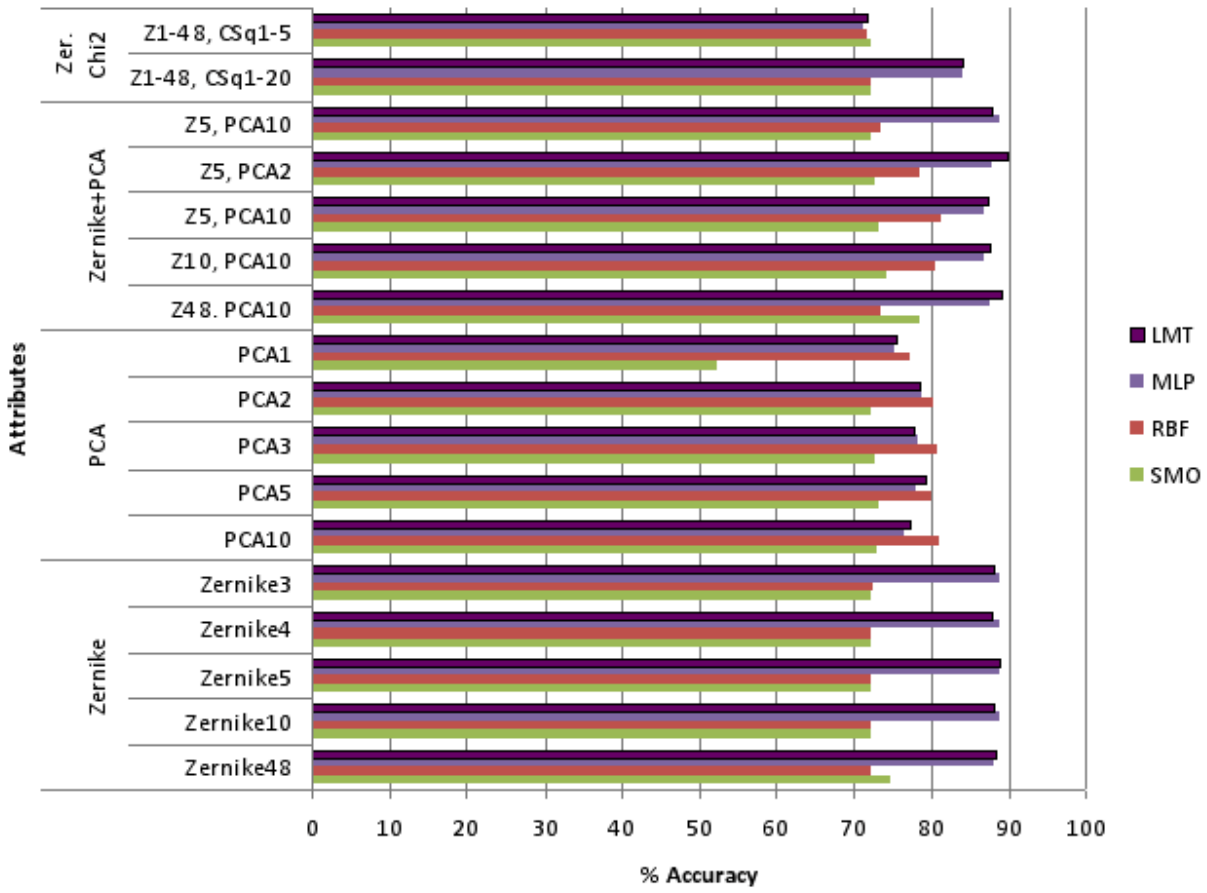

Fig. 4.11: Comparison of classifiers accuracy among the different attributes selection.

4.6 ***Conclusions***

As an essential part of the fruit grading system, the stem-end/calyx detection subsystem is the responsible for distinguishing a calyx from a defect.

After acquiring the image, it is necessary to improve the quality of the picture and identify the regions of interest (*ROI*) by removing the background and identifying the regions where the different views of the orange are present when using the mirror capture system.

Then, we segment the images into calyx candidate regions using k-means clustering over the CIE L*a*b* color space, and once we have all the candidate regions, we use Zernike polynomials and perform Principal Component Analysis to extract the features to be used in the calyx classification step.

Although the amount of descriptors retrieved might seem excessive, the data mining algorithms should discard the less significant attributes, and we also experiment using features subset selection algorithms in order to keep only the most significant attributes and compare the classification results using different datasets containing different combinations of features.

After the dataset is built, we perform the classification of candidate regions as calyxes or defects, using machine learning algorithms like Logistic Model Tree, Multilayer perceptron network with backpropagation, Sequential minimal optimization for support vector machine and Radial basis function network.

The results of the experiments show that both Logistic Model Tree and Multilayer Perceptron neural network achieve very good accuracy (89.87% for LMT and 88.89% for MLP) and a very good AUC value (0.93 for LMT and 0.92 for MLP) when processing datasets with the first 5 Zernike moments and the first two and one principal components respectivly.

The Radial Basis Function Network achieves the highest accuracy (81.05%) when processing a dataset with only principal components. However, its performance decreases significantly when using a dataset which contains only Zernike moments.

SMO shows very poor results, with a maximum accuracy of only 78.66% achieved when using the dataset with the 48 Zernike moments and the first 10 principal components.

The comparison of all the classifiers analyzed using the different data sets are shown in Table 4.3 and Figure 4.11.

Based on the obtained results, the chosen classifier for us would be the Logistic Model Tree, because of its high accuracy across the different attributes configuration, and also because of the easier interpretation of the model compared to neural networks. According to the bibliography, one of the disadvantages of this classifier is the high computational cost for real time applications [42], that is not analyzed in this thesis but should be considered in a future work because of the real time requirements of fruit grading production lines.

The obtained accuracy (89.87%) can be compared to results of similar researches performed by other authors. Unay and Gosselin [10] classify apple's calyx/stem-end with 81% accuracy when using a KNN classifier and 90.5% accuracy using SVM. Ruiz et. al [34] achieve 93% accuracy when classifying stem, calyx and leaves against skin and background in oranges using Bayesian decision rules.

5. QUALITY CATEGORIES CLASSIFICATION

The quality classification subsystem is one of the main parts of the orange grading system. Its input is the output of the calyx detection subsystem, consisting of the original image captured by the image capture subsystem, already pre-processed and mirror segmented and with the calyx removed. The purpose of this step is to process the image in order to describe that picture as a series of features that are used by the data mining algorithms in the classification step to classify the orange into one of the three pre-established categories.

This chapter is one of the most relevant parts of this thesis.

A diagram of the Input-Process-Output is shown in Figure 5.1, which shows that the input to the classification algorithms is a dataset containing the features extracted, and the output of the process is the classification result.

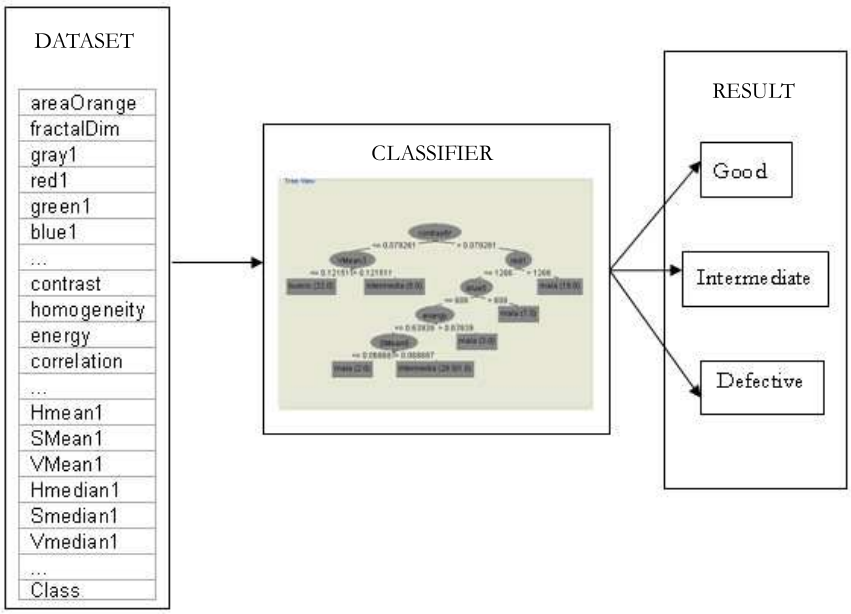

Fig. 5.1: Input-Process-Output diagram of the system where features are extracted, processed and classified

The quality categories classification subsystem is further divided into the following steps:

- Feature extraction
- Classification

Pre-processing and segmentation tasks have already been described in section 4.1 and no further pre-processing or segmentation is needed at this step.

A diagram of this process can be seen in Figure 5.2.

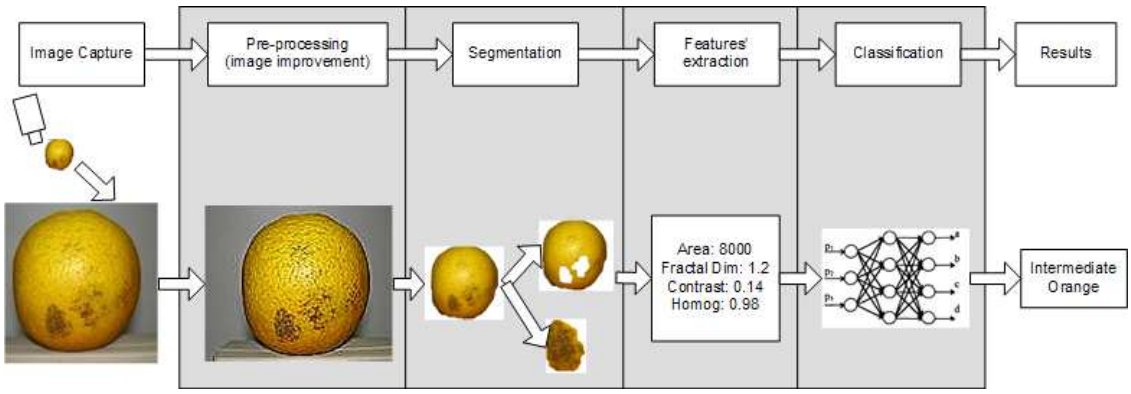

Fig. 5.2: Image processing steps.

5.1 ***Feature extraction***

In this section, the features obtained are the area of the orange and the background, the fractal dimension of region I_o, the contrast, gray level uniformity, gray level correlation between neighbours, histogram, and the mean and median calculated in the HSV color space.

The data mining algorithms used in the classification step should automatically detect the most relevant attributes (features) needed to perform the classification, discarding the rest. Therefore, in the feature extraction step we gather as many descriptors as we can in order to make classification algorithms more effective.

Next we explain in detail each one of the features extracted.

- **Orange area:** The area of the orange A_o is calculated as the sum of the pixels belonging to the orange: $A_o = \sum_{i=1}^{144} \sum_{j=1}^{192} f(i,j)$, where $f(i,j) = \begin{cases} 1 & \text{if } (i,j) \in I_n \\ 0 & \text{in other case} \end{cases}$

  We also calculate the complement descriptor (background area) A_b.

- **Fractal dimension analysis:**

  The fractal dimension FD of a set in $\mathbb{R}^n$, is a real number which characterizes its geometrical complexity, and can be used as an irregularity indicator of a set [27, 54]. The FD is defined for self-similar sets, and in the case of sets which do not have this property, the FD has to be estimated [57].

  One of the methods proposed in [27] to estimate FD and characterize the smoothness level in a section of an image is the *box-counting* dimension. This method is commonly used because it exhibits a good balance between computation time and

accuracy. However, this estimation has the inconvenient that can only be applied to binary images.

The *box-counting* dimension of a planar set A consists of estimating how changes the quantity of cells in which the set has no null measure, as function of the size of those cells.

Being $N_l(A)$ the quantity of cells of side l where the set has no null measure, the *box-counting* dimension DB of A is

$$DB = \lim_{l \to 0} \frac{\log(N_l(A))}{\log(\frac{1}{l})}, \tag{5.1}$$

if the limit exists. In practice, for finite resolution images, l has superior and inferior limits, and DB can be estimated with the slope of the minimum square regression that approximates the logarithmic diagram $\log(N_l(A)) vs. \log(\frac{1}{l})$.

Given a binary image, it is partitioned in cells of side l, and for different values of l, the quantity $N_l(A)$ of cells in which the object of interest (foreground) has no null measure is calculated. Except the case in which $l = 1$, for all l, it is necessary to make many partitions of the image and calculate $N_l(A)$ as the average. Then, DB is estimated as the minimum square regression slope previously mentioned.

To be able to apply this method it is necessary to transform the image to binary, so a thresholding process has to be applied for this purpose. In this thesis, in order to obtain the texture of the peel of the fruit to estimate the fractal dimension, we start from a gray level image of the orange with the background removed, and apply a border detection procedure with the Canny [13] algorithm, getting the image I_{can}. Then, the box counting dimension DB is calculated over the image I_{can}. A result of 1 means that the texture of the orange's peel is smooth, which means that it is a good quality orange. In the opposite side, for greater imperfections, the value of the estimator DB tends to increase.

Table 5.1 shows the results of the border detection with the Canny algorithm, and the fractal dimension obtained for a good quality orange and a defective quality one, where it can be seen that the value of DB in the good orange is lower (tending to 1) than in the defective one.

- **Texture analysis using statistical descriptors:** For the texture analysis we use six statistical descriptors, which use a co-occurrences gray level matrix. This is made calculating the number of adjacent pixel repetitions with the same gray level in the whole image.

  The statistical descriptors used are:

  - **Contrast:** The global contrast of the image (also known as variance or inertia) measures the contrast intensity between a pixel and its neighbour. Its calculation is based on the corresponding co-occurrences matrix.

	Good orange	Defective orange
Original image		
Border detection	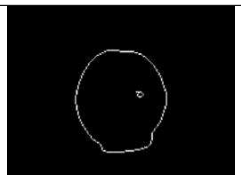	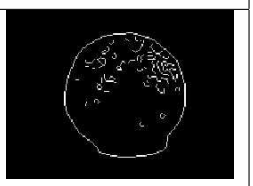
Fractal Dimension	1.0887	1.2688

Tab. 5.1: Steps in the estimation of the fractal dimension

- **Correlation:** Measures the relation of a pixel and its neighbour. The degree in which if the gray level of a pixel increases, its neighbour also increases.
- **Energy:** Also known as 'uniformity', 'energy uniformity' and 'second angular moment', consists of the sum of the squared elements in the co-occurrences matrix taken by pairs.
- **Homogeneity:** It is a value that measures the closeness of the distribution of elements of the co-occurrences matrix to the main diagonal of that matrix.
- **Skewness:** It is a measure of the degree of asymmetry of a distribution around the mean. It is obtained by calculating the third standardized central moment of the distribution. If the obtained value is zero, it means that it is centered (like the normal distribution). If it is positive, it is asymmetrical to the right, and if it is negative, to the left [22].
- **Kurtosis:** Measures how distant is the distribution of the data to the normal distribution. Is the result of calculating the fourth standardized central moment of a distribution. The kurtosis of the normal distribution is 3. A value greater than 3 (platykurtic) means that the distribution is flatter (with thicker tails), and a distribution with kurtosis less than 3 (leptokurtic) means the opposite (thiner tails and a sharp peak) [22].

A comparison of the values of these statistical descriptors of a good and defective orange are shown in Table 5.2

- **Histograms analysis:** We analyze the histograms of the red H_r, green H_g, blue H_b, and the gray levels H_{gray} histograms. A RGB histogram example can be seen in Figure 5.3. To simplify the analysis, we divide the histograms in six bins. For example, for the red component, the first bin is the amount of pixels in the image which values belong to the interval $[0, \frac{255}{6})$, the second bin $[\frac{255}{6}, \frac{255}{6} \times 2)$ and so on until the six intervals are covered.

	Good orange	Defective orange
Original image		
Contrast	0.1553	0.2852
Correlation	0.9796	0.9787
Energy	0.6097	0.4265
Homogeneity	0.9862	0.9506
Skewness	-1.32509	-0.5779
Kurtosis	2.812565	1.3816

Tab. 5.2: Texture analysis features comparison

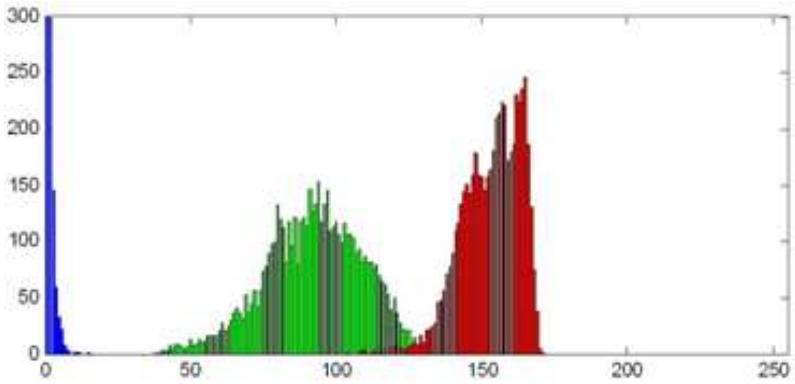

Fig. 5.3: Histogram analysis of the Red, Green and Blue components of an orange image

- **Mean and median analysis in the HSV color space:** We take color values in the region of a circumscribed rectangle inside the orange region. This rectangle is divided into smaller regions forming a grid, and for each box several measures are taken.

  For this experiment, we use a grid of 3 rows and 3 columns, and for each row the mean and median of each of the 3 components of the HSV color space are calculated, getting a total of 54 attributes. This process can be seen in Figure 5.4, and a comparison of the values obtained for the sixth position of the grid is shown in Table 5.3.

  The HSV color space is used based on the good results reported in [35].

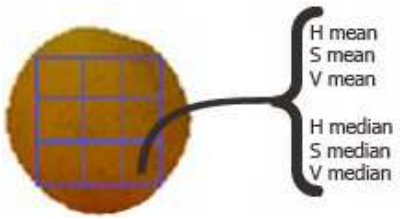

Fig. 5.4: Region of the image used to extract the mean and median features of the HSV color space.

	Good orange	Defective orange
Original image		
Hue Mean	0.0349	0.0622
Saturation Mean	0.4982	0.7904
Value Mean	0.8044	0.3713
Hue Median	0.0590	0.0572
Saturation Median	0.9434	0.7931
Value Median	0.6588	0.3529

Tab. 5.3: HSV mean and median features comparison. Hue ranges from 0 (0°=red) to 1 (360°), saturation ranges from 0 (unsaturated) to 1 (fully saturated), and value ranges from 0 (black) to 1 (brightest)

5.2 ***Classification Results***

For this experiment we use a data set obtained after processing a total of 892 oranges' images, which contains 314 high quality oranges' images, 473 intermediate quality oranges' images and 105 defective quality oranges' images. For each specimen, we extract the 95 previously described features, which are all numerical attributes. The class assignment was done manually by the authors, based on visual features and on expert's advise.

When analyzing the results, we perform a cost sensitive evaluation, since the cost of misclassifying a defective orange as a good orange is much higher than misclassifying a good orange as defective, because if a good orange is classified as defective, the revenue obtained by selling the fruit as a lower category will be lower than selling it as a good one. However, if a defective orange is sold as good, it is sold at a higher price, but when the buyer finds out that defective oranges have been sold as good, he can demand the seller to pay a fine and he will likely not buy anymore products.

The cost-matrix used is shown in Table 5.4.

Predicted class / True class	Good	Intermediate	Defective
Good	0	1	2
Intermediate	2	0	1
Defective	5	2	0

Tab. 5.4: Cost-Matrix

- **Results obtained with a J48 decision tree:** After training a J48 decision tree with the described dataset, the decision tree shown in Figures 5.7 a) and 5.5 is generated. It can be seen that the attribute $fractalDim$ (the fractal dimension) is in the root of the tree. This means that this is the best attribute to differentiate between classes.

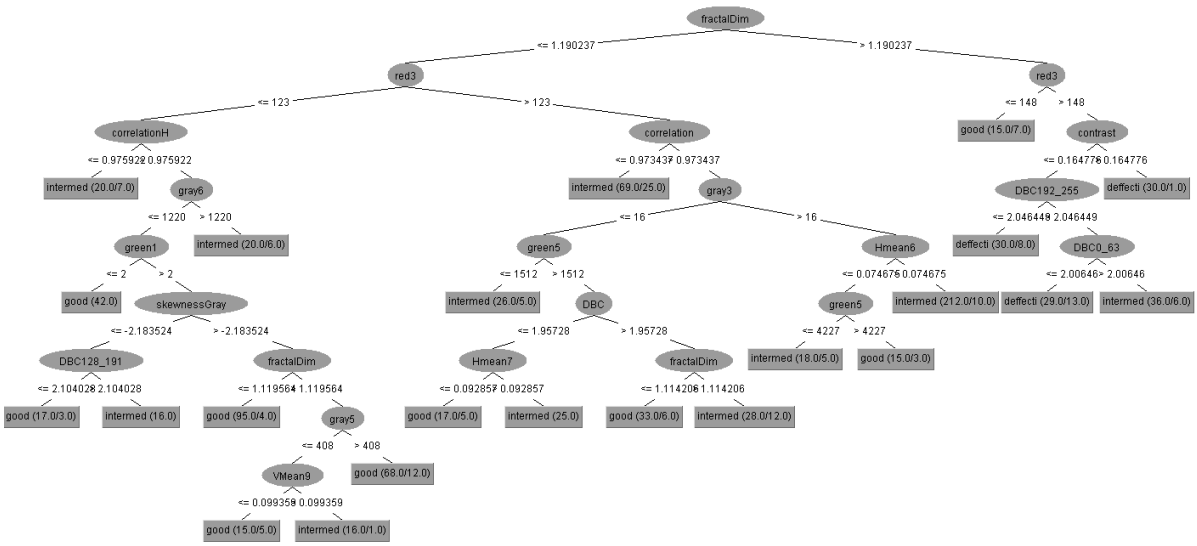

Fig. 5.5: J48 Decision tree

As it can be seen in the confusion matrix shown in Table 5.6, the accuracy achieved by the classifier is 71.08%. From all of the classification errors we obtain, there are 4 good oranges misclassified as defective, and 2 defective oranges misclassified as good. The rest of the misclassifications are between the 'intermediate' class and the others, thus the cost is 420.

We also trained a decision tree with the same configuration but using only two classes ('good' and 'defective') from the original dataset. The obtained decision tree is shown in Figure 5.6, where it can be seen that it contains the fractal dimension attribute as root node. This classifier achieves a 94.75% accuracy and an area under the ROC curve of 0.93, as it can be seen in the confusion matrix shown in Table 5.5.

Fig. 5.6: J48 decision tree for only two classes: 'good' and 'defective'.

- **Results obtained with a Best First decision tree:** Figure 5.7 b) shows the model generated by the Best First algorithm. In the root node it has the third bin of the red histogram, and other discriminant attributes are the histograms of the green and gray components of the RGB color space and the fractal dimension. The accuracy of this model is 72.20% and the total cost is 398 (see Table 5.6).

- **Results obtained with a Logistic Model Tree (LMT):** The model built with the LMT algorithm achieves an accuracy of 81.73%, and as it can be seen in the confusion matrix shown in Table 5.6, it does not commit any classification mistake between 'good' and 'defective' classes. Thus, with its cost being the lowest one with 252, it is the best model obtained for classifying oranges in three classes.

- **Results obtained with a Random Forest decision tree:** The accuracy obtained with this tree is 73.54%. Analyzing the confusion matrix, we notice that there is only one error between the 'good' and 'defective' classes, but there are many errors between the 'intermediate' and other classes, having a cost of 368.

- **Results obtained with a Simple CART decision tree:** This decision tree achieves an accuracy of 72.76% and a cost of 383 (see Table 5.6), creating a model similar to the one obtained with the Best First algorithm (see Figure 5.7 b)), as it has the third bin of the red histogram as the root element, and has the fractal dimension and the histograms of the green and gray components of the RGB color space among other discriminant attributes.

a) J48

```
fractalDim <= 1.190237
|   red3 <= 123
|   |   correlationH <= 0.975922: intermed (20.0/7.0)
|   |   correlationH > 0.975922
|   |   |   gray6 <= 1220
|   |   |   |   green1 <= 2: good (42.0)
|   |   |   |   green1 > 2
|   |   |   |   |   skewnessGray <= -2.183524
|   |   |   |   |   |   DBC128_191 <= 2.104028: good (17.0/3.0)
|   |   |   |   |   |   DBC128_191 > 2.104028: intermed (16.0)
|   |   |   |   |   skewnessGray > -2.183524
|   |   |   |   |   |   fractalDim <= 1.119564: good (95.0/4.0)
|   |   |   |   |   |   fractalDim > 1.119564
|   |   |   |   |   |   |   gray5 <= 408
|   |   |   |   |   |   |   |   VMean9 <= 0.099359: good (15.0/5.0)
|   |   |   |   |   |   |   |   VMean9 > 0.099359: intermed (16.0/1.0)
|   |   |   |   |   |   |   gray5 > 408: good (68.0/12.0)
|   |   |   gray6 > 1220: intermed (20.0/6.0)
|   red3 > 123
|   |   correlation <= 0.973437: intermed (69.0/25.0)
|   |   correlation > 0.973437
|   |   |   gray3 <= 16
|   |   |   |   green5 <= 1512: intermed (26.0/5.0)
|   |   |   |   green5 > 1512
|   |   |   |   |   DBC <= 1.95728
|   |   |   |   |   |   Hmean7 <= 0.092857: good (17.0/5.0)
|   |   |   |   |   |   Hmean7 > 0.092857: intermed (25.0)
|   |   |   |   |   DBC > 1.95728
|   |   |   |   |   |   fractalDim <= 1.114206: good (33.0/6.0)
|   |   |   |   |   |   fractalDim > 1.114206: intermed (28.0/12.0)
|   |   |   gray3 > 16
|   |   |   |   Hmean6 <= 0.074675
|   |   |   |   |   green5 <= 4227: intermed (18.0/5.0)
|   |   |   |   |   green5 > 4227: good (15.0/3.0)
|   |   |   |   Hmean6 > 0.074675: intermed (212.0/10.0)
fractalDim > 1.190237
|   red3 <= 148: good (15.0/7.0)
|   red3 > 148
|   |   contrast <= 0.164776
|   |   |   DBC192_255 <= 2.046449: deffecti (30.0/8.0)
|   |   |   DBC192_255 > 2.046449
|   |   |   |   DBC0_63 <= 2.00646: deffecti (29.0/13.0)
|   |   |   |   DBC0_63 > 2.00646: intermed (36.0/6.0)
|   |   contrast > 0.164776: deffecti (30.0/1.0)
```

b) BFTree

```
red3 < 131.0
|  green5 < 1042.5
|  |  red3 < 16.0: good(47.0/12.0)
|  |  red3 >= 16.0: intermed(43.0/27.0)
|  green5 >= 1042.5: good(167.0/33.0)
red3 >= 131.0
|  fractalDim < 1.19042
|  |  gray3 < 23.5
|  |  |  green5 < 1695.5: intermed(50.0/19.0)
|  |  |  green5 >= 1695.5
|  |  |  |  DBC < 1.96616
|  |  |  |  |  VMean7 < 0.09423: good(12.0/5.0)
|  |  |  |  |  VMean7 >= 0.09423: intermed(29.0/2.0)
|  |  |  |  DBC >= 1.96616: good(39.0/25.0)
|  |  gray3 >= 23.5
|  |  |  Hmean5 < 0.07167: good(16.0/15.0)
|  |  |  Hmean5 >= 0.07167: intermed(208.0/16.0)
|  fractalDim >= 1.19042
|  |  gray5 < 2.5
|  |  |  fractalDim < 1.20863: deffecti(6.0/4.0)
|  |  |  fractalDim >= 1.20863: deffecti(30.0/0.0)
|  |  gray5 >= 2.5
|  |  |  fractalDim < 1.25802
|  |  |  |  DBC < 1.9595: deffecti(15.0/6.0)
|  |  |  |  DBC >= 1.9595
|  |  |  |  |  fractalDim < 1.20052: deffecti(6.0/5.0)
|  |  |  |  |  fractalDim >= 1.20052
|  |  |  |  |  |  Hmean5 < 0.10536: intermed(8.0/5.0)
|  |  |  |  |  |  Hmean5 >= 0.10536: intermed(30.0/1.0)
|  |  |  fractalDim >= 1.25802: deffecti(10.0/1.0)
```

c) Simple CART

```
red3 < 131.0
|  green5 < 1042.5
|  |  red3 < 16.0: good(47.0/12.0)
|  |  red3 >= 16.0: intermed(43.0/27.0)
|  green5 >= 1042.5: good(167.0/33.0)
red3 >= 131.0
|  fractalDim < 1.19042: intermed(332.0/104.0)
|  fractalDim >= 1.19042
|  |  gray5 < 2.5: deffecti(36.0/4.0)
|  |  gray5 >= 2.5
|  |  |  fractalDim < 1.25802
|  |  |  |  DBC < 1.9595: deffecti(15.0/6.0)
|  |  |  |  DBC >= 1.9595: intermed(42.0/13.0)
|  |  |  fractalDim >= 1.25802: deffecti(10.0/1.0)
```

Fig. 5.7: Decision trees and classification rule models.

- **Results obtained with a Multilayer Perceptron Neural Network with Backpropagation:** The network consists of 95 nodes in the input layer (one for each attribute), 3 in the output layer (3 classes), and 48 in the hidden layer. The accuracy (76.68%) and cost (346) obtained are shown in Table 5.6.

  If the same neural network is trained but considering only two classes (good and defective), we obtain as a result an accuracy of 97.37% with an area under the ROC curve (AUC) of 0.99. This can be seen in Table 5.5.

- **Results obtained with a Radial Basis Function Network:** The model obtained with this algorithm achieves the worst accuracy among all the classifiers tested, with a value of 61.32%. The cost produced is also the worst with 631.

- **Results obtained with a Sequential Minimal Optimization for Support Vector Machines Network:** This network produces very good results, because it reaches an accuracy of 79.15% without any classification error between the good and defective classes, leading to a cost of 303.

- **Results obtained with a One Rule classification rule:** The One Rule classification rule achieves a very bad accuracy of 65.58% and a cost of 514.

Results obtained using a neural network with previous attribute selection:

After analyzing the results of the neural networks using the complete set of attributes for training, we decide to try three multilayer perceptron networks using datasets which have been previously reduced in the amount of attributes by the methods previously explained in section 2.2.6.

- **Correlation based feature subset selection method:** We apply the Correlation based feature subset selection evaluator together with the Best First search algorithm. The Best First search algorithm performs a greedy hill-climbing with backtracking over the attribute space [40]. As a result, we obtain that the most significant attributes are the fractal dimension, the box counting dimension, the first range of the green component, the third range of the gray histogram, the third range of the red component histogram, the fifth range of the blue component histogram, the homogeneity and correlation of the hue component of the HSV color space.

  When using this subset with the multilayer perceptron neural network, we obtain the confusion matrix shown in Table 5.6, where it can be seen that the classifier accuracy (75.67%) decreases slightly compared to the results obtained when using all the available attributes (76.68%), but the computational time used to build the model is reduced 40 times (from 269 seconds when using all the attributes to 6.7 seconds when using 20 attributes) because there are less attributes involved.

- **Chi Squared Attribute Evaluator for features subset selection:** When applying Chi Squared Attribute Evaluator together with the Ranker method, which

performs a ranking over the most significant attributes, we obtain that the fractal dimension, contrast, the third range of the red component histogram, the box counting dimension, the third range of the gray component histogram, and the homogeneity are the most significant attributes.

The resulting confusion matrix can be seen in Table 5.6, where it shows that the percentage of correctly classified instances is 78.81%, but it classifies one good orange as defective. However, its cost of 294 is very good.

- **Information Gain attribute evaluation:** With the Information gain attribute evaluator, we obtain the best results when using a multilayer perceptron neural network, with an accuracy of 79.48%. However, it classifies one defective orange as good. Even though, it produces the second lowest cost of 293. The most significant attributes are the third range of the red component, the fractal dimension, the third range of the gray component, the box counting dimension, the first range of the red component histogram, the contrast and homogeneity.

Algorithm	Predicted class / True class	Good	Defective	Accuracy	AUC
J48 2 classes	Good	303	11	94.75%	0.93
	Defective	11	94		
MLP 2 classes	Good	309	5	97.37%	0.99
	Defective	6	99		

Tab. 5.5: Orange classification results considering only two classes: Good and Defective

Algorithm	Predicted / True class	Good	Inter.	Defective	Accuracy	% Avg.	Cost
J48	Good	238	72	4	75.8%	71.08%	420
	Intermediate	97	346	30	73.2%		
	Defective	2	47	56	53.3%		
BFTree	Good	233	81	0	74.2%	72.20%	398
	Intermediate	95	355	23	75.1%		
	Defective	2	47	56	53.3%		
LMT	Good	258	56	0	82.2%	**81.73%**	**252**
	Intermediate	52	403	18	85.2%		
	Defective	0	37	68	64.8%		
Random Forest	Good	218	96	0	69.4%	73.54%	368
	Intermediate	68	394	11	83.3%		
	Defective	1	60	44	41.9%		
Simple Cart	Good	235	77	2	74.8%	72.76%	383
	Intermediate	85	359	29	75.9%		
	Defective	1	49	55	52.4%		
Multilayer Perceptron	Good	254	60	0	80.9%	76.68%	346
	Intermediate	91	360	22	76.1%		
	Defective	4	31	70	66.7%		
RBF Network	Good	224	88	2	71.3%	61.32%	631
	Intermediate	162	271	40	57.3%		
	Defective	23	30	52	49.5%		
SMO	Good	250	64	0	79.6%	**79.15%**	**303**
	Intermediate	53	415	5	87.7%		
	Defective	0	64	41	39.0%		
1R	Good	207	105	2	65.9%	65.58%	514
	Intermediate	79	378	16	79.9%		
	Defective	7	98	0	0.0%		
MLP with CfsSubset Eval	Good	258	56	0	82.2%	75.67%	394
	Intermediate	98	361	14	76.3%		
	Defective	10	39	56	53.3%		
MLP with Chi Squared	Good	258	55	1	82.2%	**78.81%**	**294**
	Intermediate	75	369	29	78.0%		
	Defective	0	29	76	72.4%		
MLP with Information Gain	Good	263	51	0	83.8%	**79.48%**	**293**
	Intermediate	76	372	25	78.6%		
	Defective	1	30	74	70.5%		

Tab. 5.6: Orange grading results

5.3 *Conclusions*

Once the segmentation process is finished, we apply several image processing techniques to obtain several descriptors of that image, like area, fractal dimension, texture statistical descriptors, color descriptors from histogram analysis, and statistical descriptors from the HSV color space.

Then, in the classification step we apply nine data mining algorithms for orange quality classification through visual features. The first group of algorithms are decision trees (J48, Best First, Logistic Model Tree, Random Forest and Simple CART), the second group consists of neural networks (Multilayer Perceptron, Radial Basis Function and Sequential Minimal Optimization) and then a classification rule (1Rule) is analyzed.

The main advantage of decision trees and classification rules over neural networks are their simplicity and interpretation of the obtained classification rules, as neural networks work as a black box and the model produced by the algorithm are much more difficult to interpret.

Although most of the algorithms produce good results (with an accuracy higher than 75%), the Logistic Model Tree, Sequential Minimal Optimization neural network and Multilayer perceptron neural network with attribute selection are the ones which, in the experiments done, produce the models with the highest accuracy (about 80%). Most of the errors produced by the SMO algorithm are defective oranges misclassified as intermediate ones (64 errors) and good oranges misclassified as intermediate ones (64 errors), while the Logistic Model Tree misclassifies 56 good oranges as intermediate, 52 intermediate as good and other misclassifications between intermediate and defective classes.

One of the drawbacks of SMO is that only 39% of the defective oranges are classified as such, while with the LMT 64.6% of the defective oranges are correctly classified, and with the Multilayer perceptron with attribute subset selection using Information Gain, 70.5% of the oranges are correctly classified. However, MLP with Information Gain misclassifies one defective orange as good.

Analyzing the results, we choose the Logistic Model Tree as the best classifier, because not only it achieves the highest classification accuracy (81.73%) and the lowest cost (252), but also the model produced by a Logistic Model Tree is easier to interpret by humans compared to the one produced by the Multilayer perceptron and SMO neural networks.

On the opposite side, the algorithms with the worst accuracy are the Radial Basis Function Network (61.32%), which misclassifies 23 defective oranges as good and 2 good as defective, and the One Rule algorithm (65.58%), which misclassifies 2 good oranges as defective and 7 defective as good.

6. CONCLUSIONS AND FUTURE WORKS

In the food industry, quality assurance processes can benefit from automated visual inspection, because it provides a uniform way of performing the classification, and free the workers from the repetitive task of visually inspecting one by one all the harvested fruit.

Performing an accurate classification is crucial in order to fulfill the quality requirements established by several organizations to allow the commercialization of the fruits for specific markets. If a good quality orange is misclassified as defective or intermediate, it will be sold at a lower price, but if a defective orange is misclassified as good, it might lead to the application of fines for selling defective oranges as good; or if the defect is an illness, it can lead to discard the whole lot of fruits, causing a considerable loss of money.

The development of an automated orange grading system is not a trivial task, as the defects found in the fruits can be of very different types and do not usually exhibit a known pattern. Thus, they cannot be detected using conventional image processing techniques.

One of the most difficult tasks faced in fruit grading systems is the detection of the calyx, which is necessary in order not to misclassify the calyx as a defect. A wrong detection of the calyx would reduce the overall accuracy of the orange grading system, either if it detects a calyx where in fact is a defect which will classify a defective orange as good, or if it does not detect the calyx, downgrading the obtained category.

Along this thesis we have proven the feasibility of building an automatic orange grading system using data mining and image processing techniques.

The process starts by capturing images from all possible angles using an inspection chamber with a digital camera and a set of mirrors. Then, the background is removed and a segmentation step which uses k-means clustering over the CIE L*a*b* color space detects the candidate regions where it is likely to find a calyx. Next, Zernike Moments and Principal Components features are extracted in order to build a dataset to be used in the classification step to classify the region as a defect or a calyx. In this step, we compare several machine learning algorithms, choosing the Logistic Model Tree as the best classifier, because of its high accuracy across the different datasets and attributes configuration, and also because of the easier interpretation of the model compared to the neural networks.

Next, the quality categories classification subsystem receives as an input the image of the orange with its calyx removed, where several geometric, textural and statistical features are extracted, being the fractal dimension, the contrast attribute of the HSV color

space, the third range of the red component histogram and the fifth range of the green component histogram some of the most relevant features obtained. With these features, in the classification step we build a dataset and apply several machine learning algorithms, being the Logistic Model Tree, Sequential Minimal Optimization neural network and Multilayer Perceptron neural network with Backpropagation the classifiers which achieve the best classification rates.

Most of this work can also be applied to classifying other kinds of fruit, specially citrus. However, several adjustments should be done depending on the color, shape, texture and other features of the fruit. Also, the data mining algorithms should be retrained in order to learn the new kind of problem. We intend to analyze the application of the system to other types of fruits in a future research.

Another area we are interested in is to classify the detected defects into different categories of defects and identify illnesses.

In a future work, we will optimize the processing speed of the algorithms. To do this, it will be necessary to measure the amount of oranges classified in a certain amount of time, like for example the amount of oranges classified per second. This will be done taking into account the speed requirements of real production lines.

We are also interested in implementing in the future the image capture subsystem and classified oranges placement subsystem in order to integrate all the hardware and software components and be able to test the whole orange grading system in real production lines.

BIBLIOGRAPHY

[1] Gholamreza A., Ali E., George B., and Mircea N. Accurate and efficient computation of high order Zernike moments. In *ISVC*, pages 462–469, 2005.

[2] Khotanzad A. and Hong Y. H. Invariant image recognition by Zernike moments. *IEEE Trans. Pattern Anal. Mach. Intell.*, 12(5):489–497, 1990.

[3] Palak K. A. and Koduvayur P. S. Rotation and cropping resilient data hiding with Zernike moments. In *ICIP*, pages 2175–2178, 2004.

[4] Wiliem A., Vamsi K., Wageeh B., and Prasad Y. A face recognition approach using Zernike moments for video surveillance. In *RNSA Security Technology Conference*, Melbourne, Australia, 2007.

[5] Wiliem A., Vamsi M., Wageeh B., and Prasad Y. Eye detection in facial images using Zernike moments with SVM. In *RNSA Security Technology Converence 2007, School of Engineering Systems, Queensland University of Technology*, pages 341–355, Melbourne, Australia, 2007.

[6] Galiano F. B. *ART: Un método alternativo para la construcción de árboles de decisión.* PhD thesis, Departamento de Ciencias de la Computación e Inteligencia Artificial, Ingeniería Informática, Universidad de Granada, 2002.

[7] Caiafa C. and Proto A. N. Desarrollo de un software para la identificación de elefantes marinos por eigenfaces. In *Reportes Técnicos en Ingeniería del Software*, volume 5, pages 27–40. CAPIS-EPG-ITBA, 2003.

[8] Jensen D. and Cohen P. Multiple comparisons in induction algorithms. *Machine Learning*, pages 309–338, 1997.

[9] Mery D. Inspección visual automática. In *Actas del 1er Congreso Internacional de Ingeniería Mecatrónica*, Lima, Perú, 2002.

[10] Unay D. and Gosselin B. Apple defect detection and quality classification with MLP-Neural Networks. In *International workshop ProRISC 2002 (Circuits, Systems and Signal Processing)*, 2002.

[11] Unay D. and Gosselin B. Stem-end/calyx detection in apple fruits: Comparison of feature selection methods and classifiers. In *Proc. Int. Conf. Computer Vision and Graphics (ICCVG)*, 2004.

[12] Johnson D. E. *Métodos multivariados aplicados al análisis de datos*. International Thomson Editores, 1998.

[13] Canny F. A computational approach to edge detection. *IEEE-PAMI*, 8(6):679–698, 1986.

[14] López F., Valiente J. M., and Caselles R. B.and Vanrell M. Fast surface grading using color statistics in the CIE Lab space. *Lecture Notes in Computer Science*, 3523:666–673, 2005.

[15] Provost F., Fawcett T., and Kohavi R. The case against accuracy estimation for comparing induction algorithms. In *In Proceedings of the Fifteenth International Conference on Machine Learning*, pages 445–453. Morgan Kaufmann, 1997.

[16] Jan H. and Kamber M. *Data Mining: Concepts and Techniques.* Morgan Kaufmann, 2000.

[17] Zubrzycki H. and Molina. Factibilidad comercial de cítricos entre Argentina y Brasil. In *Publicación de la EEA Bella Vista Serie Técnica N^o 17*, 2005.

[18] Witten I. and Frank E. *Data Mining: Practical Machine Learning Tools and Techniques. Second Edition*. Morgan Kaufmann, 2005.

[19] Hertz J., Krogh A., and Palmer R. *Introduction to the Theory of Neural Computation*. Wesley Publishing Co., 1991.

[20] Xing J., Jancsok P., and Baerdemaeker J. Stem-end/calyx identification on apples using contour analysis in multispectral images. *Biosystems engineering*, pages 231–237, 2007.

[21] B. Jahne. *Digital Image Processing: Concepts, Algorithms, and Scientific Applications*. Springer-Verlag New York, Inc., Secaucus, NJ, USA, 1997.

[22] D. N. Joanes and C. A. Gill. Comparing measures of sample skewness and kurtosis. *Journal of the Royal Statistical Society: Series D (The Statistician)*, 47(1):183–189, 1998.

[23] Mercol J.P. and Gambini M. J. Stem-end/calyx detection in oranges using image processing and data mining techniques. *XIII Reunión de trabajo en Procesamiento de la Información y Control (RPIC)*, pages 141–146, September 2009.

[24] Mercol J.P., Gambini M. J., and Santos J. M. Clasificación automática de naranjas por medio de imágenes utilizando técnicas de data mining. *Jornadas Chilenas de Computación 2008*, 2008.

[25] Mercol J.P., Gambini M. J., and Santos J. M. Automatic classification of oranges using image processing and data mining techniques. *XIV Congreso Argentino de Ciencias de la Computación*, October 2008.

[26] Erum A. K. and Erik R. A survey of color spaces for shadow identification. In *APGV '04: Proceedings of the 1st Symposium on Applied perception in graphics and visualization*, pages 160–160, New York, NY, USA, 2004. ACM.

[27] Falconer K. *Fractal Geometry: Mathematical Foundations and Applications*. John Wiley & Sons, Chichester, England, 1990.

[28] Forbes K. *Volume estimation of fruits from digital profile images*. PhD thesis, Department of Electrical Engineering, University of Cape Town, Cape Town, 2000.

[29] Hyoung-Joon K. and Whoi-Yul K. Eye detection in facial images using Zernike moments with SVM. *ETRI Journal*, 30(2):335–337, Apr. 2008.

[30] Breiman L. Random forests. *Machine Learning*, 45(1):5–32, 2001.

[31] Breiman L., Friedman J.H., Olshen R.A., and Stone C J. *Classification and Regression Trees*. Wadsworth Publishing Company, Belmont, California, USA, 1984.

[32] Jin C. L., Ling C. X., Huang J., and Zhang H. AUC: a statistically consistent and more discriminating measure than accuracy. In *In Proceedings of 18th International Conference on Artificial Intelligence (IJCAI-2003)*, pages 329–341, 2003.

[33] López-Conejo L. and Sánchez-Yánez R. Segmentación de imágenes naturales usando el espacio de color CIE Lab. *III Encuentro Participación de la Mujer en la Ciencia*, May 2006.

[34] Ruiz L.A., Molto E., Juste F., Pla F., and Valiente R. Location and characterization of the stem-calyx area on oranges by computer vision. *Journal of Agricultural Engineering Research*, 64:165–172(8), July 1996.

[35] Fernández Ribot M. *Selector de fruta y simulación de una aplicación real*. PhD thesis, Universidad Politécnica de Catalunya, España, 2006.

[36] Mitchell T. M. *Machine Learning*. McGraw-Hill, 1997.

[37] Recce M., Taylor J., Plebe A., and Tropiano G. High speed vision-based quality grading of oranges. In *NICROSP '96: Proceedings of the 1996 International Workshop on Neural Networks for Identification, Control, Robotics, and Signal/Image Processing (NICROSP '96)*, pages 136–144, Washington, DC, USA, 1996. IEEE Computer Society.

[38] Servente M. and García Martinez R. Algoritmos TDIDT aplicados a la mineria de datos inteligentes. *Revista Del Instituto Tecnológico de Buenos Aires*, 26:39–57, 2002.

[39] Twa M., Parthasarathy S., Rosche T., and Bullmer M. Decision tree classification of spatial data patterns from videokeratography using Zernike polynomials. *SIAM International Conference on Data Mining*, 2003.

[40] Hall M.A. and L. A. Smith. Feature subset selection: A correlation based filter approach. In *Conf. on Neural Information Processing and Intelligent Information Systems*, pages 855–858, Hamilton, New Zealand, 1997. Springer (Ed.).

[41] Donald Michie, D. J. Spiegelhalter, C. C. Taylor, and John Campbell, editors. *Machine learning, neural and statistical classification*. Ellis Horwood, Upper Saddle River, NJ, USA, 1994.

[42] Landwehr N., Hall M., and Frank E. Logistic model trees. In *Machine Learning*, pages 241–252. Springer-Verlag, 2003.

[43] Marques N. and Chen N. Border detection on remote sensing satellite data using Self-Organizing Maps. In *Pires F.M., Abreu S.(Eds.): EPIA 2003, LNAI 2902. Spinger-Verlag Berlin Heidelberg.*, pages 294–307, 2003.

[44] N. Nilsson. *Introduction to Machine Learning*. MIT Press (to appear), 1998.

[45] D'Amato J. P., García B. C., Vénere M., and Clausse A. Procesamiento de imágenes para la clasificación masiva de frutos basado en el color. In *Universidad Nacional del Centro, CNEA-CICPBA-CONICET*, 2007.

[46] Gay P., Berruto R., and Piccarolo P. Fruit color assessment for quality grading purposes. In *ASAE Annual International Meeting/ CIGR XVth World Congress*, pages 28–31, Chicago, Illinois, USA, 2002.

[47] J. C. Platt. *Fast training of support vector machines using sequential minimal optimization*. MIT Press, Cambridge, MA, USA, 1999.

[48] Kohavi R. A study of cross-validation and bootstrap for accuracy estimation and model selection. In *IJCAI*, pages 1137–1145, 1995.

[49] González R.C., Woods R., and Eddins S. *Digital Image Processing Using MATLAB*. Pearson Prentice-Hall, 2004.

[50] Holte R.C. Very simple classification rules perform well on most commonly used datasets. *Mach. Learn.*, 11(1):63–90, 1993.

[51] Haijian S. Best-first decision tree learning. Master's thesis, University of Waikato, Hamilton, NZ, 2007. COMP594.

[52] Haykin S. *Neural Networks. A Comprehensive Foundation Second Edition*. Prentice Hall International Inc, 1999.

[53] Carg A. Sebe N., Cohen I. and Huang T. *Machine Learning in Computer Vision*. Springer, 2005.

[54] Chen S.S., Keller J.M., and Crownover R.M. On the calculation of fractal features from images. *Pattern Analysis and Machine Intelligence*, 15(10):1087–1090, 1993.

[55] Fawcett T. ROC graphs: Notes and practical considerations for researchers. *Kluwer Academic Publishers*, 2004.

[56] Morimoto T., Takeuchi T., Miyata H., and Hashimoto Y. Pattern recognition of fruit shape based on the concept of chaos and neural networks. *Computers and Electronics in Agriculture*, pages 171–186, 2000.

[57] Liu Y. and Li Y. Image feature extraction and segmentation using fractal dimension. In *International Conference on Information and Signal Processing*, pages 975–979, Singapur, 1997. IEEE.